Development of a Restricted Simplex for Optimizing Force Constants in Normal Coordinate Calculations and Applications to SERS Spectra

by

Alberto L. Vivoni

A dissertation submitted to the Graduate Faculty in Chemistry in partial fulfillment of the requirements for the degree of Doctor of Philosophy, The City University of New York

1995

This manuscript has been read and accepted for the Graduate Faculty in Chemistry in satisfaction of the dissertation requirement for the degree of Doctor of Philosophy.

12-9-71	
Date	Chair of Examining Committee
Aug 7, 1975	
Date	Executive Officer
	Thomas C Stree
	Ronald A Bieke
	Supervisory Committee

THE CITY UNIVERSITY OF NEW YORK

Abstract

Development of a Restricted Simplex for Optimizing Force Constants in Normal Coordinate Calculations and Applications to SERS Spectra

by

Alberto L. Vivoni

Advisor: Professor Ronald L. Birke
Professor John R. Lombardi

A restricted simplex method was developed to optimize force constants in normal coordinate calculations. The method keeps the normal modes from crossing over each other by requiring that the normal mode assignments are obeyed during iterations. A description of the method and results of pyrimidine, aniline and flavin calculations are presented. The method is compared with other methods of obtaining force constant values and evaluated on the basis of frequency and isotopic shift match and the reasonableness of the calculated force constants. The method was applied to the SERS spectra of ammonia, pyridine, adenine and NAD^+. The frequency shifts between the solution and SERS spectra were reproduced by perturbing the force field obtained from solution

calculations. The accuracy of the calculation method allowed one to obtain information about the interaction between the molecule and the surface such as orientation of the molecule on the surface, charge re-distribution and structural changes. The method was also applied to 4-atoms clusters. Quantum mechanical calculations of rhomboidal Si_4 were reproduced and the force fields of tetrahedral P_4, Ta_4 and Bi_4 were calculated.

Table of Contents

List of Tables

List of Illustrations

Chapter I: Introduction

1.1 Overview

Wilson, Deicus and Cross popularized normal coordinate calculations with their GF method.[1] These authors developed a system for expressing the kinetic and potential energies in matrix forms that could be applied to any molecule. But diagonalizing the GF matrix analytically restricted the method to molecules of no more than 6 atoms. Years later, Schachtschneider wrote a set of normal coordinate calculation programs based on the Wilson method.[2] Diagonalization programs made it feasible to calculate the normal modes of large molecules. However, since the force constants were estimated on a trial and error basis, obtaining their right values remained a problem. Optimization programs improved the method in this respect. But they also brought new problems into the procedure. Random variation of the force constants caused normal modes to cross-over each other.[3] One could thus obtain an excellent frequency fit but with the wrong assignments. This thesis project involved developing a method to solve the crossing-over problem and applying it to a number of normal mode calculations. Chapter II describes the method developed. There, some sample calculations are

presented and results evaluated by comparison with other methods.

The motivation for improving the normal coordinate calculations was to help interpret surface enhanced Raman scattering (SERS) spectra.[4] The interactions between molecules and the surface of the electrode used in the SERS experiment cause changes to the Raman spectra. Fine tuning the calculations would allow one to probe into the mechanisms of these interactions. Chapter III describes the application of the method developed for ammonia and pyridine adsorbed on the electrode surface. The information obtained from the calculations presented in chapters II and III helped interpret the adenine and NAD^+ SERS spectra. Chapter IV presents the SERS spectral analysis of these two molecules. Finally, in chapter V, the method developed is applied to 4-atoms clusters.

Numerous books explain normal coordinate theory in detail.[5-8] The next section describes only that part of the theory which is needed to understand the method developed. The simplex optimization will also by explained summarily afterward.

1.2 Normal Coordinate Theory

The potential energy expression used in normal coordinate theory is derived from its Taylor series expansion

$$V(q_1, q_2, \cdots, q_{3N}) = V_0 + \sum_{i}^{3N}\left(\frac{\partial V}{\partial q_i}\right)_0 q_i + \frac{1}{2}\sum_{i,j}^{3N}\left(\frac{\partial^2 V}{\partial q_i \partial q_j}\right)_0 q_i q_j + \cdots \qquad (1)$$

For convenience, mass weighted Cartesian coordinates are used in the calculation. These are defined as

$$q = m^{-1/2} \cdot x$$

where m is the atomic mass and x is the equilibrium Cartesian coordinate. The first term on the right hand side of the equation (1) is a constant and is discarded. The second term, the first derivative of the potential energy at equilibrium position, is zero and is also discarded. The third and higher order terms do not contribute significantly to the shape of the curve and are therefore ignored. We are thus left with

$$2V = \sum_{i,j}^{3N} f_{ij} q_i q_j \qquad (2)$$

the simple harmonic potential function. The force constants are then defined as

$$f_{ij} = \frac{\partial^2 V}{\partial q_i \partial q_j}$$

This expression is directly related to the force constant of Hook's law for a system of two masses attached by a spring.

The kinetic energy in mass weighted Cartesian coordinates is expressed as

$$2T = \sum_{i,\,j}^{3N} (\dot{q}_i)^2 \qquad (3)$$

Plugging equations (2) and (3) into Lagrange's equation of motion

$$\ddot{q} + \sum_{j}^{3N} f_{ij} q_j = 0$$

and after some matrix manipulations[8] we end up with a system of homogeneous linear equations

$$\sum_{i}^{3N} (f_{ij} - \delta_{ij}\lambda) A_i = 0$$

This equation is composed of the force constant matrix, f, the eigenvalues, λ, and unknown amplitude coefficients A_i. It has

$$\left| f_{ij} - \delta\lambda \right| = 0$$

as its non-trivial solution. The vibrational secular equation is then

$$\begin{vmatrix} f_{11}-\lambda & f_{12} & f_{13} & f_{14} & \cdots & f_{1,3N} \\ f_{21} & f_{22}-\lambda & f_{23} & f_{24} & \cdots & f_{2,3N} \\ f_{31} & f_{32} & f_{33}-\lambda & f_{34} & \cdots & f_{3,3N} \\ \cdot & & & & & \\ \cdot & & & & & \\ \cdot & & & & & \\ f_{3N1} & f_{3N,2} & f_{3N,3} & f_{3N,4} & \cdots & f_{3N,3N}-\lambda \end{vmatrix} = 0$$

With the procedure described above, the normal coordinate calculation has been reduced to one of diagonalizing the force constant matrix. The result yields the eigenvalues, related to the frequencies, and eigenvectors, related to relative atomic displacement vectors. The normal mode of vibration is one of the 3N solutions with

$$\upsilon_k = \sqrt{\lambda / 2\pi}$$

where all the atoms of the mode vibrate with the same frequency, υ_k.

The most useful way to express the force constant matrix is in internal coordinates. This system of coordinates represents the motions of the atoms in terms of bond stretches and angle deformations. In water, for example,

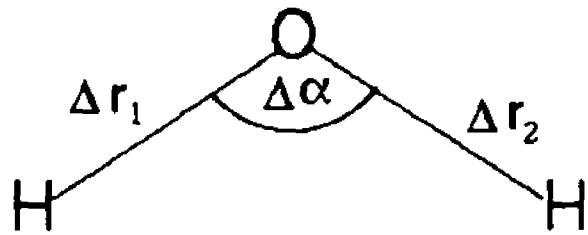

the internal coordinates Δr_1 and Δr_2 are the displacements of the atoms along the direction of the O-H bonds. $\Delta\alpha$ expresses the displacement of the atoms along the H-O-H angle deformation coordinate.

The potential energy in internal coordinates is written as

$$2V = \mathbf{R}^t \mathbf{F} \mathbf{R}$$

For water,

$$2V = [\Delta r_1 \Delta r_2 \Delta\alpha] \begin{bmatrix} f_{11} f_{12} f_{13} \\ f_{21} f_{22} f_{23} \\ f_{31} f_{32} f_{33} \end{bmatrix} \begin{bmatrix} \Delta r_1 \\ \Delta r_2 \\ \Delta\alpha \end{bmatrix}$$

Expanding this expression one obtains

$$2V = f_{11}(\Delta r_1)^2 + f_{11}(\Delta r_2)^2 + f_{33}(\Delta\alpha)^2 + 2f_{12}(\Delta r_1)(\Delta r_2) + 2f_{13}(\Delta r_1)(\Delta\alpha) + 2f_{13}(\Delta r_2)(\Delta\alpha) \quad (4)$$

The diagonal terms in the force constant matrix correspond to the force constants of the internal coordinates and the off-

diagonals to interactions between these. By symmetry for H_2O, $f_{11}=f_{22}$, $f_{12}=f_{21}$ etc.

Two types of force fields may be used to express the force constants, valence bond and Urey-Bradley.[9] Equation (4) is the valence bond force field potential energy for water. In this expression, each force constant may take on independent values. In the Urey-Bradley force field, the off-diagonal terms are determined by non-bonded interactions, Δq.

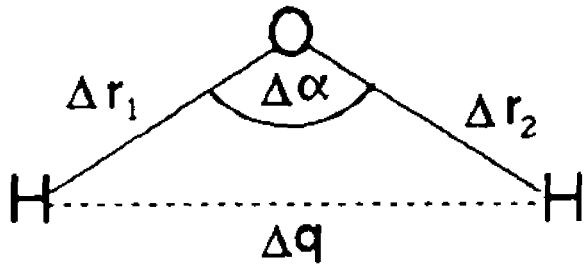

The general form of the Urey-Bradley potential energy[10] is given by

$$V = \sum_i \left(\frac{1}{2}K_i(\Delta r_i)^2 + K'_i r_i(\Delta r_i)\right) + \sum_i \left(\frac{1}{2}H_i r_{i\alpha}^2(\Delta\alpha)^2 + H'_i r_{i\alpha}^2(\Delta\alpha)\right) + \sum_i \left(\frac{1}{2}F_i(\Delta q_i)^2 + F'_i q_i(\Delta q_i)\right)$$

The relation between the Urey-Bradley and valence bond force constants are obtained using

$$q_{ij}^2 = r_i^2 + r_j^2 - 2r_i r_j \cos\alpha_{ij}$$

and are given by

$$f_{11} = K + t^2F' + s^2F$$
$$f_{33} = H - s^2F' + t^2F$$
$$f_{12} = - t^2F' + s^2F$$
$$f_{13} = ts(F' + F)$$

where

$$s = \frac{r(1 - \cos \alpha)}{q}$$

$$t = \frac{r \sin \alpha}{q}$$

The advantages and disadvantages of each force field will be discussed in the following chapters.

1.3 Simplex Optimization Method

The simplex method is generally used in numerical analysis for curve fitting.[11] It works by searching for the minimum on a curve fitting surface. For n number of parameters, it evaluates a function with n+1 sets of parameters, each set corresponding to a vertex with coordinate vectors $\mathbf{P}_1$, $\mathbf{P}_2$, ..., $\mathbf{P}_j$, ..., $\mathbf{P}_n$, $\mathbf{P}_{n+1}$. The program compares the error of all sets and discards one that yields the worst function evaluation, say $\mathbf{P}_j$. It then draws a new

vertex by one of many possible operations such as reflection through the centroid, $\bar{\mathbf{P}}$, of the hyperface normal to the discarded vertex, where

$$\bar{\mathbf{P}} = (1/n)(\mathbf{P}_1 + \mathbf{P}_2 + \ldots + \mathbf{P}_n + \mathbf{P}_{n+1}).$$

The new vertex, $\mathbf{P}_j^*$, is obtained from

$$\mathbf{P}_j^* = \bar{\mathbf{P}} + (\bar{\mathbf{P}} - \mathbf{P}_j).$$

In the case of normal coordinate calculations, the points being fitted correspond to experimental frequencies. Figure 1.1 shows a two dimensional simplex. In this example, $\mathbf{P}_1$ produced the worst frequency fit. The program discards this vertex and draws $\mathbf{P}^*$ from it. The process is repeated until the best fit is obtained.

Figure Caption

Figure 1.1 Representation of a two-dimensional simplex.

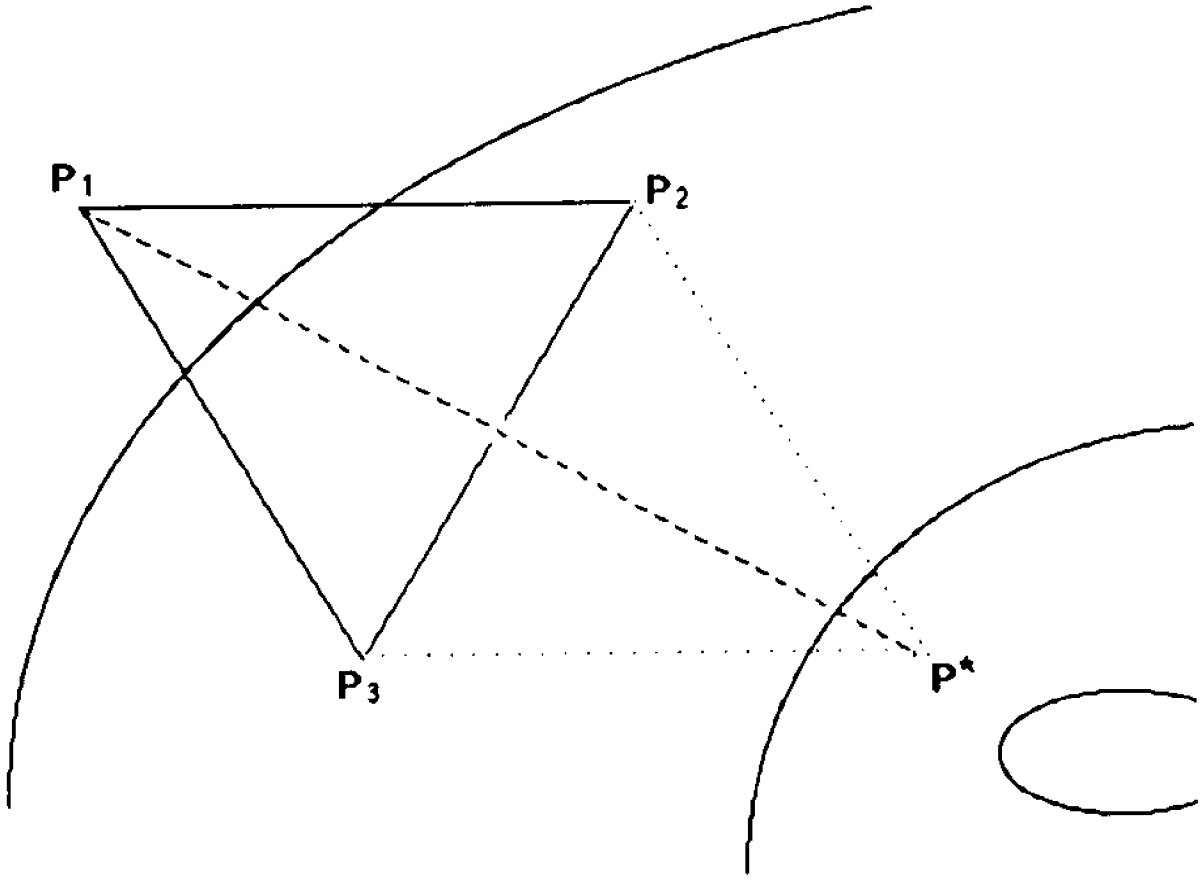

Figure 1

Chapter II: Development of a Restricted Simplex for Optimizing Force Constants in Normal Coordinate Calculations with Applications to Aniline, Pyrimidine and Flavin.

2.1 Introduction

One of the most difficult things about a normal mode analysis is calculating the force field. To help in this endeavor, one invokes the transference approximation.[1-4] This approximation suggests that bond stretches and angle deformations with the same type of atoms should have similar values. Normal coordinate calculations have been historically a build-up procedure. The force fields of complex molecules were obtained by transferring the force constants from simpler molecules.[5-7] Calculations of methane, for example, provided many of the force constants for the methane substituted molecules. These in turn, provided many of the force constants for larger substituted hydrocarbons. After the initial estimate, the force constants are refined to fit the known band assignments and improve the frequency match. Refining the force constants by manually varying them can be a monumental task. Here, again, the transference approximation helps. It indirectly sets limits on the force constant values. Nevertheless, the procedure is still

cumbersome and time consuming, especially for large molecules.

To expedite the normal mode calculation procedure and eliminate its tediousness, we developed an automated method to optimize the force constants. This was done by adapting a Nelder-Mead simplex--after some modifications--to a set of normal coordinate calculation programs.[8] Least squares and simplex methods have been used before in force constant refinements.[9,10] However, these methods bring other problems into the procedure.[11,12] In a random variation of parameters, the frequencies may cross over each other yielding wrong band assignments and physically unreasonable force constants. Other researchers have addressed these problems by restricting the range in which a force constant may be varied during the iterations.[13] This method insures that the force constants do not stray too much, but the frequencies may still cross over. Another problem with this method is that empirical formulas for deformation force constants have not been as carefully studied as for the stretching force constants. In the method presented here, we attack the problem from the side of the frequency assignments. We keep the normal modes from crossing over each other by pre-assigning those frequencies whose assignments are known from experiment, to specific force constants. We call this a restricted simplex method. The imposed restrictions also keep the force constants within reasonable values. In addition to the restrictions, this method has the advantage over the

General Vibrational Analysis Programs from the Quantum Chemistry Exchange Program of allowing for both valence bond and Urey-Bradley force field calculations.[9]

2.2 Method

Our Nelder-Mead simplex fitting routine is a FORTRAN 77 program which has generally been used in numerical analyses for curve fitting. It works by searching for the minimum in a curve fitting error surface. The simplex searches for the minimum by evaluating an n parameter function with n+1 sets of parameters, each set corresponding to a vertex with coordinate vectors $\mathbf{P}_1$, $\mathbf{P}_2$,..., $\mathbf{P}_j$,..., $\mathbf{P}_n$, $\mathbf{P}_{n+1}$ and comparing the error of all sets. The program then discards the worst set of parameters, say $\mathbf{P}_j$, and draws a new vertex by a variety of means one of which is reflecting through the centroid, $\bar{\mathbf{P}}$, of the hyperface normal to the discarded vertex. $\bar{\mathbf{P}}$ is obtained from the following formula

$$\bar{\mathbf{P}} = (1/n)(\mathbf{P}_1 + \mathbf{P}_2 + \ldots + \mathbf{P}_n + \mathbf{P}_{n+1}).$$

The new vertex, $\mathbf{P}_j^*$, is obtained from

$$\mathbf{P}_j^* = \bar{\mathbf{P}} + (\bar{\mathbf{P}} - \mathbf{P}_j).$$

For the purpose of refining the force constants in normal coordinate calculations, a Nelder-Mead simplex from *Numerical Recipes* was added to the set of normal coordinate programs from Diem[14,15] who modified the ones originally written by Schachtschneider.[16] The set consists of four programs: CART.FOR, BMAT.FOR, UBZM.FOR and NOCO.FOR. CART.FOR calculates the Cartesian coordinate matrix, **x**, from bond lengths and bond angles. BMAT.FOR calculates the **B** matrix which transforms between Cartesian and internal coordinates **R**

$$\mathbf{R} = \mathbf{B}\,\mathbf{x}.$$

UBZM.FOR calculates the **Z** matrix. This matrix assigns a force constant value to the internal coordinates in the **F** matrix

$$\mathbf{F} = \mathbf{Z}\,F\ .$$

F is a one dimensional matrix where the force constants are entered. The force constants may be entered for a Urey-Bradley or a valence bond force field. When using a valence bond force field, UBZM.FOR assigns the values to the force constant matrix directly from input file. When using a Urey-Bradley force field, UBZM.FOR calculates the scaling factors of the off-diagonal elements according to the type of non-bonded interaction specified in the input file. The NOCO.FOR program diagonalizes the force constant matrix which yields the eigenvalues, λ, and the eigenvectors **C**. The program also

converts the eigenvalues to wave numbers and calculates the average percentage error between the calculated and observed frequencies. The restricted simplex compares the results of each iteration on the basis of the average percentage error.

NOCO.FOR also calculates the potential energy distribution (PED) and the atomic displacement vectors **S**. The atomic displacement vectors are obtained from

$$\mathbf{S} = \mathbf{M}^{-1/2}\ \mathbf{C}$$

where **M** is the atomic mass matrix and **C** the eigenvector matrix of the force constant matrix. **C** is expressed in mass weighted Cartesian coordinates **q**

$$\mathbf{q} = \mathbf{M}^{-1/2}\ \mathbf{x}.$$

The PED shows the changes in the potential energy of all the internal coordinates for each normal mode in terms of the force constants. It is calculated *via* the **L** matrix which transforms from internal coordinates to normal coordinates, **Q**,

$$\mathbf{R} = \mathbf{L}\ \mathbf{Q}$$

and is calculated by

$$\mathbf{L} = \mathbf{B}\ \mathbf{S} = \mathbf{B}\ \mathbf{M}^{-1/2}\ \mathbf{C}.$$

In terms of the components of the **L** matrix, the eigenvalues of each normal mode, λ_i, may be expressed as

$$\lambda = \sum_{j,i} L_{ji} L_{ki} F_{jk}$$

The ratio $L_{ji}L_{ki}F_{jk}/\lambda_i$ then represents the fractional contribution of each force constant to a particular normal mode. Detailed description of normal coordinates methods may be obtained from references.[17-19]

The simplex was programmed to check the pre-assignment conditions on the resulting PED of each iteration. The conditions require that the main contributing force constant be consistent with the bands assignments. That is, for a normal mode with eigenvalue, λ_i, assigned to m vibrational mode, the fractional contribution of F_{mm} should be the largest of all F_{jk},

$$L_{ji}\ L_{ki}\ F_{mm}\ /\ \lambda_i\ >\ L_{ji}\ L_{ki}\ F_{jk}\ /\ \lambda_i$$

for m, $m \neq j, k$. For example, from deuterium substitution, one determines the hydrogen deformation modes on the vibrational spectra. In the PED of those modes, the hydrogen bending force constants will have the largest fractional contribution. While the force constants vary during the optimization, other modes with different PED's may cross-over the hydrogen deformation modes. By imposing the conditions mentioned above, the hydrogen bending force constant remains

the main contributing force constant to the hydrogen deformation modes and inhibits the crossing over. An arbitrary value of 10 is added to the average percentage error of any iteration that does not meet the conditions. Since the average percentage error is normally less than 5 %, a 10 % or more is discarded by the simplex as a worst value. Figure 2.1 shows the output of NOCO.FOR for methyl chloride-excluding the atomic displacement vectors-after a restricted simplex optimization. The observed frequencies were obtained from Overend and Sherer.[4] In the PED, one sees that the main contribution to the 1354.9 cm^{-1} band comes from the Cl-C-H bending, *i.e.* the combination of H(Cl-C-H) and F(Cl..H). By pre-assigning the 1354.9 cm^{-1} band to H(Cl-C-H) and F(Cl..H) combined, one blocks the 1454.6 cm^{-1} band with a large H(H-C-H) contribution from crossing over it. Figure 2.2 compares the first 20 iterations of simplex optimizations with and without restrictions for methyl chloride. At this stage, the 1454.6 cm^{-1} and 1354.9 cm^{-1} bands crossed over in the non-restricted simplex optimization and lowered the average percentage error of the frequency fit. Without the conditions, the non-restricted simplex could not asses the path its was lead through by this "improvement" on the frequency fit and was thus lead astray. The optimizations from figure 2.2 were started with an artificially high average percentage error for the purpose of illustrating the effects of the restrictions.

The restricted simplex runs while the frequency fit improves. The convergence criterion is specified in the input files and is determined by the difference between the best two iteration results. The program is set to restart automatically to allow the simplex search to move out of a local minimum on the curve fitting surface. A convergence criterion for the number of simplex runs is also specified in the input files. Figure 2.3 shows the subsequent iterations of the optimizations in figure 2.2. The added value of 10 for the iterations that do not meet the conditions are not shown. The non-restricted simplex restarted at 100 iterations and stopped at 200. At this point, the symmetric and anti-symmetric cross over blocked any further improvement of the frequency fit. The cross-over also showed on the deuterated methyl chloride calculation. The restricted simplex restarted at 180 and 340 iterations. Enforcing the frequency assignments with the restrictions allowed the simplex to reduce the average percentage error to 0.1 %. The force constants obtained in this matter reproduced the right assignments of deuterated methyl chloride. The average percentage error on the deuterated species was 1.12 %. The simplex allows one to include up to 5 isotopic species in the optimization. Running the program with methyl chloride and its deuterated species would have yielded a more balanced frequency fit. As mentioned earlier, the optimization was started at an artificially high percentage error. A better set of initial force constants avoided the cross-over when

using a non-restricted simplex. This is normally the case for small molecules like methyl chloride. However, molecules of more than 10 atoms show cross-over even when starting with an average percentage error below 3 %.

We designed four ways to pre-assign the normal modes: 1) to the highest contributing force constant, 2) to the second highest, 3) to the first and second highest, 4) to the highest contributing group. Which way is used depends on the circumstances. The first way is used for cases where a band assignment is clearly known. The second way may be used for those normal modes that are combinations of many internal coordinates. This occurs often with bonds outside an aromatic ring such as in aniline or phenol. In this case, the x-substituted bond frequency is often known. However, the frequency usually contains large contributions from ring stretches and hydrogen deformations and the x-substituted bond stretch may not show up as the main force constant. The third way may be used for cases where the general assignment is known, but not the specific internal coordinate. For instance, in pyridine, the frequencies above 1500 cm^{-1} are known to be mostly ring stretches. However, which of the three ring stretches predominates is not apparent. The fourth way is used when the two predominant force constants are clearly known. Not all frequencies need be pre-assigned. Trial simplex runs without restrictions indicate the modes that cross-over. As the number of atoms in the molecule

increases, the number of modes that cross-over also increases.

When adjusting the force constants by trial and error, a large number of parameters is not a problem. This was the procedure followed by Abe and Kyogoku which will be discussed below.[20] However, when using an optimization routine, the ratio of the adjustable parameters to data points should be less than one. Otherwise, the iterations may diverge or yield spurious force constant values even with pre-assignments. The advantage of using a Urey-Bradley force field in a simplex optimization is that it reduces the number of independently varied parameters. When using a valence bond force field, many off-diagonal elements are set equal to zero. Except for conjugation interactions, bond stretches and angle deformations that are more than one bond away from each other are assumed to have no interaction.[21] The pyrimidine valence bond parameters from the above calculations were obtained in this manner. Even with this approximation, there is still some arbitrariness in deciding which parameters to use. The Urey-Bradley force field has the additional advantage of eliminating this arbitrariness.

To run the restricted simplex it is best to start with a good set of force constants. The closer the initial frequency fit, the less the force constants will wander about, even with the restrictions. Furthermore, the initial force field should meet all the pre-assignment conditions. In some cases, one can start without meeting the pre-assignment conditions

and the simplex will find the proper assignments. However, this procedure is not recommended because in such cases the simplex is more likely to diverge.

2.3 Results

2.3.1 *Aniline.*

For the aniline in-plane normal mode calculations, we used the experimental data from Evans.[22] This data included the frequencies of aniline, aniline-ND_2 and aniline-NDH. The Raman frequencies were used wherever they were observed; the liquid ir wherever they were not. The benzene geometry was used for the phenyl part of the molecule. The geometry of the amine group was taken from adenine. These geometrical approximations add a slight error to the calculations. This was done to show that one can obtain good results quickly starting from basic information.

The initial force field for the benzene part of the molecule was approximated from Scherer and Overend's benzene calculations.[23] The amine h-deformation force constant was initially approximated by fitting the 1618 cm^{-1} band and the deuterated shifts. Except for the NH_2 twist, Evan's band assignments were used to adjust the force constants before the optimization. Evans assigned the NH_2 twist to the 1050 cm^{-1} band. However, Tsuboi[24] determined from ^{15}N substitution that the NH_2 twist band occurred at 1115 cm^{-1}. Before the

optimization, the 1620 cm^{-1} band in aniline was pre-assigned to h-bending. Without this restriction, the ring stretches would overtake the PED. of this band.

All three aniline species could have been included in the optimization. Using all isotopomers has the advantage of insuring good isotopic shift matches. However, the deuterium deformation bands were not observed in Evans spectra. We, therefore, used only aniline. The resulting force constants were then applied to the other two species.

Table 2.1 shows the calculated and observed frequencies for aniline, aniline-NDH and aniline-ND_2. The average percentage error between the observed and calculated values was 0.80 %. All but two frequencies had relative percentage errors of more than 2.00 %: the 2483 cm^{-1} and the 522 cm^{-1} bands in aniline-ND_2. The overall agreement is excellent considering that only 14 parameters were used. The errors above 2.00 % are due to fitting 6 N-H stretching frequencies with one N-H stretch and 3 C-C-C deformation frequencies with one C-C-C bend. The PED. (not shown) agrees with Evan's assignments except for the 1115 cm^{-1} band. The simplex results show that this band is largely NH_2 twit in agreement with Tsuboi.

Evans did not report the same three normal modes in either aniline-NHD or aniline-ND_2. Our calculations show that two of these should appear between 1350 and 1300 cm^{-1}. Evans observed two frequencies close to these values. However, the atomic displacement vectors do not agree with the

depolarization ratios. The other frequency not reported by Evans was the deuterium rockings. Our calculations showed that this frequency should appear at 963 cm^{-1} in aniline-NHD and 895 cm^{-1} in aniline-ND_2. This latter one may be the band at 880 cm^{-1} reported as an out-of-plane hydrogen bend. The former was estimated by Evans at ca. 960 cm^{-1}.

2.3.2 *Pyrimidine.*

Milani-Nejad and Stidham obtained the vibrational spectra for pyrimidine and 5 deuterated species.[25] They assigned many of the bands from the symmetry of the normal mode and the product and sum rules. Pongor *et al.* changed some of the assignments of pyrimidine and pyrimidine-d_4 based on scaled quantum mechanics calculations.[26] We calculated both the Urey-Bradley and the valence bond force fields using Pongor's assignments and applied the resulting force field to the -2d, -2,5-d_2, -4,6-d_2 and -2,4,6-d_3 species. For the sake of comparison, we used the same number of force constants in both calculations

The initial Urey-Bradley force constants were transferred from Susuki and Orville-Thomas' pyridine calculations.[27] This starting force field yielded the proper symmetry assignments of the pyrimidine and pyrimidine-d_4 normal modes. The initial valence bond force field was obtained by matching the assignments obtained from the Urey-Bradley force field calculations. The modes symmetries were determined from the atomic displacement vectors. The

geometrical parameters were obtained from reference 28. The internal coordinates used are shown in figure 2.4.

Both force fields were optimized using a restricted simplex which included pyrimidine and pyrimidine-d_4. For the Urey-Bradley calculations, the 1568 cm^{-1} band was pre-assigned to the C_1-N_2 stretch. The normal mode corresponding to this frequency has B_2 symmetry. If not pre-assigned, this mode would cross over with the one at 1564 cm^{-1} which has A_1 symmetry. The 1398 cm^{-1} band was pre-assigned in pyrimidine to a ring stretch and the 1043 cm^{-1} in pyrimidine-d_4 to a ring deformation. Without the restrictions these modes crossed over the ones at 1370 and 1030 cm^{-1} respectively. In the valence bond. calculations, the only the 1043 and 1030 cm^{-1} normal modes crossed over each other.

The results of the calculations are presented in tables 2.2 and 2.3. Table 2.2 shows the fundamental bands and specifies the ones we reassigned based on the calculations. The most questionable assignments by Milani-Nejad and Stidham are the deuterium shifts of the 1065 and 992 cm^{-1} bands in -4,6-d_2, -2,4,6-d_3 and d_4. These bands are mostly ring deformation and ring stretching. Benzene and pyridine calculations show that these bands do not shift upon deuterium substitutions. Table 2.3 shows the observed and calculated shifts of the isotopic species.

Most of the reassignments were done by switching frequencies with other modes with the same symmetry. In pyrimidine-2,5-d2, however, we assigned new values not

considered fundamentals by Milani-Nejad and Stidham to two normal modes. These were the modes reported at 1325 and 910 cm^{-1}. The Urey-Bradley and the valence bond calculations yielded relative errors of 4.9 % or higher for these frequencies. These authors observed shoulders in the ir spectrum at 1435 and 845 cm^{-1} that agree better with both our force field calculations.

Only one other band from all of the species gave errors of 3.9 % or larger in both calculations. That was the 944 cm^{-1} frequency in the -2,4,6-d3 species. We, nevertheless, believe that 944 cm^{-1} is the right frequency since the 3.9 % error—although in the limit—is still an acceptable error, especially for a deuterium shift. There is not an alternate frequency in Milani-Nejad and Stidham's spectra. The band at 916 cm^{-1} in -4,6-d2 gave an error of 4.0 % in the Urey-Bradley force field calculations. However, the valence bond force field calculations gave an error of 2.0 % only. Therefore, the calculations do not contradict Milani-Nejad and Stidham's assignment.

The valence bond force field gave a slightly lower average error than the Urey-Bradley force field, 0.52 % *vs.* 0.68 %. Its optimization also converged faster and easier. Convergence of the Urey-Bradley force constants depended on the initial force constant values. The valence bond optimization converged even with force constants that were far from the minimum values. Not always is the valence bond force field more effective than the Urey-Bradley, as it was

in this case. With aniline, for example, our efforts thus far have not produced results that are comparable to those obtained with the Urey-Bradley force field.

2.3.3 *Flavin.*

Abe and Kyogoku calculated the force field of flavin using the spectra of flavin and 6 isotopomers. These authors obtained their starting force constants from calculations of similar molecules. They then improved the frequency fit by trial and error. The assignments of many frequencies were identified from isotopic substitutions of rings atoms. The assignments, in their turn, helped to determine the values of the ring stretches. The final force field included 69 force constants. It fitted satisfactorily 33 fundamental frequencies and all the isotopic shifts.

We estimated the starting force constants for the simplex run from Abe's calculations. To avoid the problems of too many parameters described above, we optimized the force constants in two ways. One was by setting all the bond stretches and angle deformations with the same kinds of atoms equal to each other. Figure 2.5 shows the internal coordinates used. The other way was to optimize the force constants by a series of steps. On one step, only the diagonal force constants were optimized; on the next step, only the off-diagonal. The process was repeated until the frequency fit did not improve further. Not all diagonal force constants were optimized since there were 41 of them. Only

those whose contribution to any normal mode was more than 5.0 % were optimized. The force constants not optimized were all ring deformations. Both ways of optimization produced frequency cross-over. Thus pre-assignment conditions were used in both cases.

Table 2.4 compares the results of the two types of optimizations with Abe and Kyogoku's results. Since Abe did not use an optimization routine, it is expected that our frequency match would be better than theirs. A fair comparison must include the isotope shift matches as well. From table 2.4 we note that a restricted simplex improves substantially the frequency fit without loss of the isotope shift match. The stepwise optimization improved the results 53.7 % and the reduced force field optimization 43.9 %.

2.4 Discussion

The transference approximation helps to estimate the initial force constant values and their range of variation. The force constant results of an optimization should, therefore, be close to the transferred values. Since our method set limits on the force constants only indirectly, we must then compare the initial and final values when evaluating the results.

Another criterion used in evaluating force constants is the physical reasonableness of the values. Several authors

have developed empirical formulas that relate the length of a bond with the magnitude of its force constants.[29] These formulas were developed by curve fitting bond length vs. force constant values from previous calculations of a wide range of molecules. All of these formulas are inspired by Badger's rule which works well for many diatomics.[30,31] In polyatomic molecules, the off-diagonal elements make the relationship less straight forward. Nevertheless, these formulas have been used successfully to estimate the starting force constant values and to define the force constants range. For evaluating our results of the C-C bonds, we used the Johnson, Burig, Dunitz formula

$$f(r) = 2300.5 \times 10^{-1.169r}$$

and Badger, Herschbach, Laurie formula

$$f(r) = 4118.4 \times 10^{-2.192r}$$

for the C-N bonds. Because of the uncertainties in the methods of obtaining the empirical formulas, differences of 10 % are acceptable when comparing their values with normal coordinate calculated values. Relationships have also been developed for bond angle.[32] However, we only use the stretching relations in our analysis since they are the more common ones.

Table 2.5 shows the Urey-Bradley force constants that were transferred from benzene and pyridine to carry out the aniline and pyrimidine calculations. The resulting force constants were converted to valence bond. values through a Z-matrix conversion. The largest differences between the transferred force constants and the final ones occurs with the hydrogen deformations. This is because the H deformations and the H non-bonded interactions complement each other. Comparing the initial with the final results one sees that as the H deformation decrease, the H non-bonded interaction increases. The complementarity can also be seen from the valence bond. converted values. These values agree, in relative terms, with the initial values where N-C-H has a higher value than the C-C-H. Table 2.5 also shows the percentage differences from the empirical formulas presented above. The pyrimidine valence bond. force constants are shown in table 2.6. In this table, the ring stretchings are compared with Pongor *et al.*'s scaled quantum mechanics values. The percentage differences from the empirical formulas are also given.

Neither we nor Abe and Kyogoku used an empirical formula to estimate the force constants in the calculations. We, therefore, thought it appropriate to use these formulas to compare the results. Figure 2.6 shows the plots of Abe and Kyogoku's results and our two optimizations results. The force constants that best fit the curves are those from the reduced field calculations. These force constants deviated

9.3 % from the formulas values. Abe and Kyogoku and the stepwise optimization deviated 10.4 % and 10.5 % respectively.

2.5 Conclusion

The above results and their comparisons show that the restricted simplex method yields accurate frequency matches without loss of isotope shift match. It also keep the force constant within reasonable values as estimated from other similar molecules or bond lengths. The restricted simplex does not completely eliminate the need for a manual refinement of the force constants. Before the optimization, band assignment conditions should be met. Neither will the simplex automatically find the right force field every time. Several trial runs may be required before obtaining satisfactory results. In spite of that, the restricted simplex is an efficient and convenient method for doing normal mode calculations. Further more, the method speeds up the calculations and makes them easier to do by eliminating the manual adjustment of the force constants.

Table 2.1. Observed and calculated frequencies in cm^{-1} of aniline and its amine-deuterated species.*

Aniline		Aniline-NHD		Aniline-ND_2	
Obs. freq.	Calc. freq.	Obs. freq.	Calc. freq.	Obs. freq.	Calc. freq.
3435	3465	3380	3413	3085	3040
3360	3354	3089	3041	3067	3036
3088	3040	3075	3036	3050	3034
3072	3036	3052	3034	3038	3032
3053	3034	3029	3032	3006	3031
3040	3032	3007	3031	2570	2575
3010	3031	2507	2498	2483	2425
1620	1644	1603	1620	1604	1616
1602	1602	1586	1600	1580	1590
1586	1585	1501	1512	1502	1496
1501	1486	1479	1470	1458	1448
1468	1459	1442	1432	-	1340
1330	1343	-	1326	-	1322
1312	1309	-	1309	1303	1307

* Observed frequencies from ref. (22).

Table 2.1. Continued

Aniline		Aniline-NHD		Aniline-ND_2	
Obs. freq.	Calc. freq.	Obs. freq.	Calc. freq.	Obs. freq.	Calc. freq.
1120	1140	1084	1075	1081	1074
1050	1058	1030	1022	1029	1022
1029	1022	999	1017	999	1017
998	1017	-	963	-	895
812	823	803	809	800	803
621	621	620	621	618	620
533	524	526	516	522	508
390	391	368	372	359	356

Table 2.2. Observed frequencies in cm^{-1} of pyrimidine isotopomers (from ref. 25) and their assignments.

$-h_4$	-2d	$-2,5-d_2$	$-4,6-d_2$	$-2,4,6-d_3$	$-d_4$
1568	1564	1536	1555	1548	1536
1564	1560	1551	1535	1535	1527
1466	1438	1435†	1446	1385	1325
1398	1393	1388	1295	1283	1275
1370	1271	1265	1305	1125*	1030
1225	944*	950*	1074*	944*	907
1159	1162*	1162*	1177*	1177*	1165
1139	1115	1109	874*	864*	860
1071	1115*	845†	916	912	820
1065	1057	1056	1061*	1045*	1043
992	990	976	989*	987*	975
678	670	664	669	665	657
623	622	618	612	610	603

* Fundamentals assigned by Milani-Nejad and Stidham to different vibrations

† Frequencies not assigned as fundamentals by Milani-Nejad and Stidham.

Table 2.3. Observed and calculated frequency shifts, in cm^{-1}, with valence bond and Urey-Bradley force fields of the pyrimidine isotopomers.*

$-h_4$	-2-d			$-2,5-d_2$		
	Obs. shift.	Calc. UB	Calc. VB	Obs. shift.	Calc. UB	Calc. VB
1568	4	16	9	17	11	9
1564	4	1	4	28	17	18
1466	28	14	45	31	54	65
1398	5	4	7	10	4	10
1370	99	98	90	105	113	96
1225	281	305	289	275	280	266
1159	-3	-22	-32	-3	-14	15
1139	24	16	11	30	24	23
1071	-44	-40	-22	226	248	251
1065	8	1	8	9	1	13
992	2	2	8	16	15	18
678	8	7	8	14	14	15
623	1	0	1	5	1	1

* Observed frequencies from ref. (25).

Table 2.3. cont.

$-h_4$	$-4,6-d_2$			$-2,4,6-d_3$		
	Obs. shift.	Calc. UB	Calc. VB	Obs. shift.	Calc. UB	Calc. VB
1568	13	10	6	20	29	19
1564	29	33	6	29	34	12
1466	20	18	16	81	67	96
1398	103	113	97	115	121	112
1370	65	88	77	245	266	246
1225	151	167	165	281	234	258
1159	-18	-28	-22	-18	-29	-30
1139	265	267	282	275	268	283
1071	155	117	140	159	178	169
1065	4	-11	8	20	-1	15
992	3	3	14	5	7	26
678	9	3	4	13	10	11
623	11	8	11	13	9	12

Table 2.3. cont.

$-h_4$	$-d_4$		
	Obs. shift.	Calc. UB	Calc. VB
1568	32	32	19
1564	37	42	24
1466	141	127	127
1398	123	125	121
1370	463	497	472
1225	195	188	203
1159	-6	-25	2
1139	279	269	283
1071	251	254	259
1065	22	4	28
992	17	17	32
678	21	16	19
623	20	9	12

Table 2.4. Frequency match and isotopic shift comparison (in cm^{-1}) between Abe and Kyogoku's results and this work's.

	Frequency match	Isotopic shift match
Abe and Kyogoku	1.73	2.38
Stepwise optimization	0.76	2.42
Reduced force field	0.93	2.48

Table 2.5. Urey-Bradley Force constants comparisons (in mdyne/Å) with initial estimates and the percentage difference from Li's empirical formulas after conversion to valence bond values through the z matrix.

Type*	This work's	Initial	Z converted	% dif. from empirical formulas
Aniline				
K(C-H)	4.56	4.79†		
K(N-H)	6.32	5.86		
K(C-C)	5.03	5.15†	6.32	
K(C-N)	5.26	5.30	7.11	
H(C-C-H)	0.29	0.36†		
H(C-C-C)	0.61	0.58†		
H(H-N-H)	0.33	0.41		
H(C-N-H)	0.63	0.52		
H(C-C-N)	0.64	0.70		
ρ	0.31	0.35†		
F(C..H)	0.40	0.32†		
F(C(N)H)	0.16	0.10		
F(C..C)	0.65	0.59†		
F(N..C)	0.41	0.36		

* K: stretching, H: bending, F: non-bonded interaction, ρ aromatic interaction.

† Values from Scherer and Overend.

Table 2.5. cont.

Type	This work's	Initial	Z converted	% dif. from empirical formulas
Pyrimidine				
$K(N_3-C_4)$	5.55	5.64	6.98	3.23
$K(N_3-C_2)$	5.32	5.64	6.72	4.40
$K(C_1-C_2)$	4.39	4.74*	5.93	5.97
H(N-C-H)	0.30	0.44	0.63	
$H(C-C_2-H)$	0.39	0.35	0.57	
$H(C-C_1-H)$	0.31	0.35	0.49	
H(C-N-C)	0.46	0.19		
H(C-C-C)	1.05	0.77*		
r	0.40	0.38		
F(N..H)	0.64	0.53		
F(C..H)	0.38	0.37		
F(N..C)	0.50	0.50		
F(C..C)	0.80	0.75*		

Table 2.6. Pyrimidine valence bond force constants (in mdyne/Å) and comparison with Pongor *et al*'s scaled quantum mechanical values and Li's empirical formula's values

Type*	This work's	Pongor *et al*.'s	% dif. from empirical formulas.
$K(N_3-C_4)$	7.21	7.12	6.75
$K(N_3-C_2)$	7.06	7.04	9.70
$K(C_1-C_2)$	6.67	6.58	5.72
H(N-C-H)	0.65		
$H(C-C_2-H)$	0.48		
$H(C-C_1-H)$	0.47		
H(C-N-C)	0.99		
H(C-C-C)	1.37		
ρ_o	0.93		
ρ_m	-0.54		
ρ_p	0.32		
$f_{rs,rb}$	0.38		
$f_{rs,hb}$	0.43		

* K: stretching; H: bending; ρ, ρ_m, ρ_p: ortho, meta and para conjugation interaction; $f_{rs,rb}$, $f_{rs,hb}$: ring stretch interacting with ring and hydrogen bend where the ring bond is part of the angle bend.

Figure Captions

Figure 2.1. Output from NOCO.FOR of methyl chloride calculation after a restricted simplex optimization.

Figure 2.2. Average percentage error of the first 20 iterations of a non-restricted simplex (solid line) and a restricted simplex (dashed line) from the optimization of methyl chloride. Iterations that did not meet the conditions are marked with an X.

Figure 2.3. Average percentage error of the iterations from the complete simplex runs from figure 1.

Figure 2.4. Deformation coordinates of pyrimidine used in the restricted simplex optimization.

Figure 2.5. Internal coordinates of flavin used in the optimization with a reduced force field: (a) stretches, (b) deformations

Figure 2.6. Plots of force constant vs. bond length of compared with Li's empirical formula. (a) Abe and Kyogoku results, (b) restricted simplex stepwise optimization, (c) reduced force field optimization.

FORCE CONSTANTS

1	4.6805	K(C-H)
2	2.0828	K(C-CL)
3	.5102	H(H-C-H)
4	.2480	H(HCCl)
5	.0240	F(H..H)
6	.5972	F(H..Cl)
7	-.0485	ρ

OBSERVED AND CALCULATED FREQUENCIES

	OBS.FREQ. (CM-1)	CALC.FREQ. (CM-1)	DIFFERENCE (CM-1)	PERCENT ERROR
1	3041.8	3041.8	0.0	0.000
2	3041.8	3041.8	0.0	0.000
3	2937.0	2934.5	2.5	.086
4	1454.6	1451.4	3.2	.218
5	1454.6	1451.4	3.2	.219
6	1354.9	1357.3	-2.4	-.180
7	1015.0	1013.8	1.2	.116
8	1015.0	1013.8	1.2	.116
9	732.1	732.1	0.0	.004

AVERAGE ERROR= 1.5 CM-1 OR .10 PERCENT.

POTENTIAL ENERGY DISTRIBUTION

OBS.FREQ = 3041.8 CALC.FREQ = 3041.8
.95 FORCE CONST # 1 K(C-H)

OBS.FREQ = 2937.0 CALC.FREQ = 2934.5
.93 FORCE CONST # 1 K(C-H)

OBS.FREQ = 1454.6 CALC.FREQ = 1451.4
.93 FORCE CONST # 3 H(H-C-H)

OBS.FREQ = 1354.9 CALC.FREQ = 1357.3
.39 FORCE CONST # 3 H(H-C-H)
.23 FORCE CONST # 4 H(HCCl)
.28 FORCE CONST # 6 F(H..Cl)

OBS.FREQ = 1015.0 CALC.FREQ = 1013.8
.34 FORCE CONST # 4 H(HCCl)
.59 FORCE CONST # 6 F(H..Cl)

OBS.FREQ = 732.1 CALC.FREQ = 732.1
.67 FORCE CONST # 2 K(C-CL)
.28 FORCE CONST # 6 F(H..Cl)

Figure 2.1

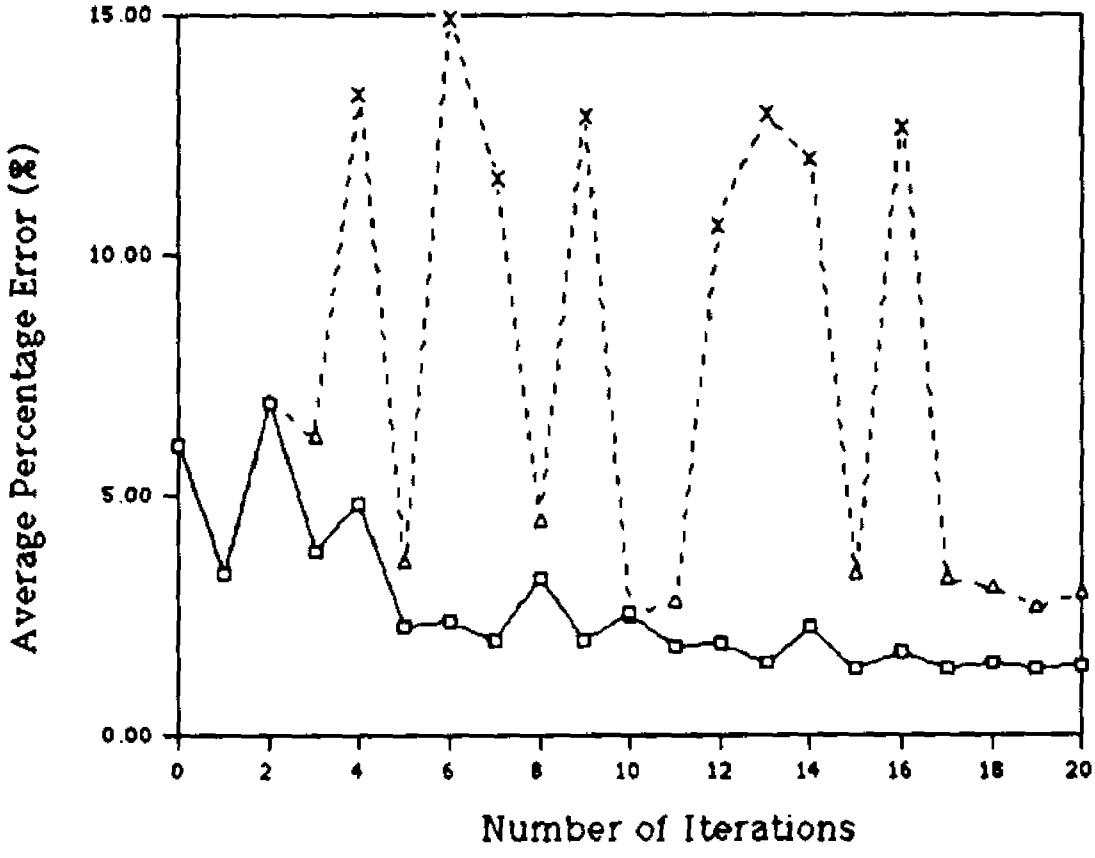
15.00
10.00
5.00
0.00
Average Percentage Error (%)
0
2
4
6
8
10
12
14
16
18
20
Number of Iterations

Figure 2.2

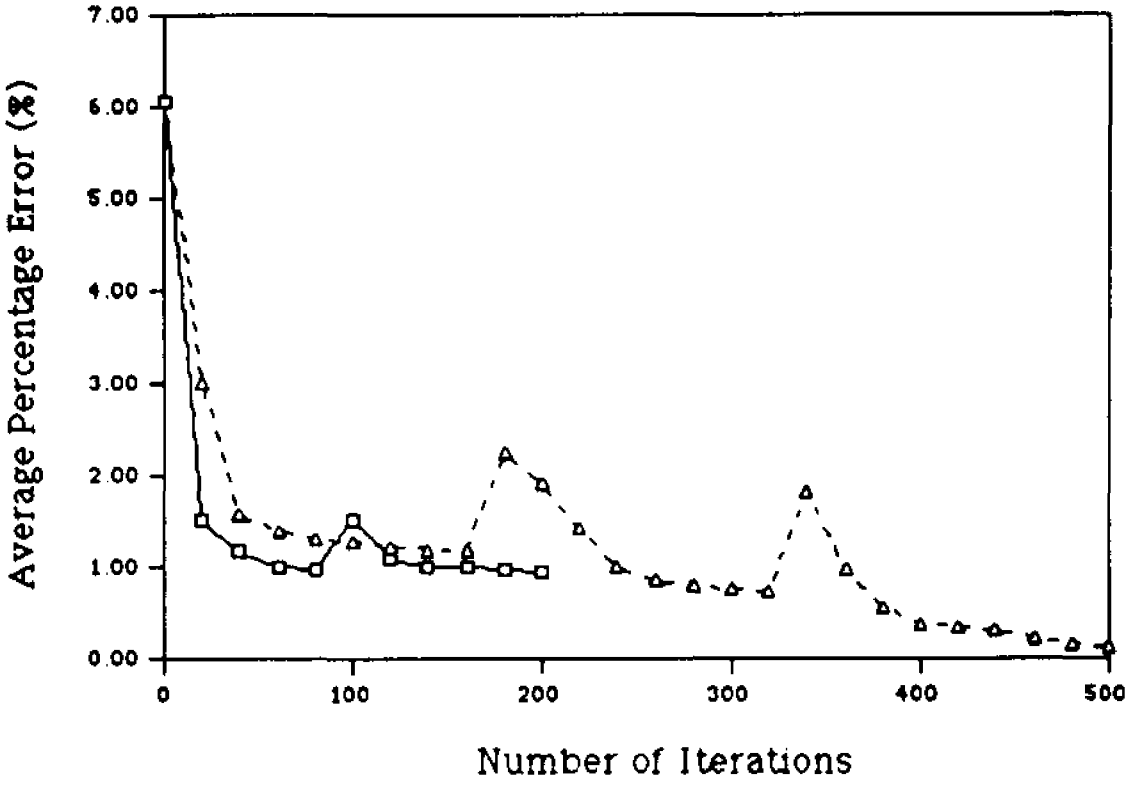
7.00
6.00
5.00
4.00
3.00
2.00
1.00
0.00
Average Percentage Error (%)
0
100
200
300
400
500
Number of Iterations

Figure 2.3

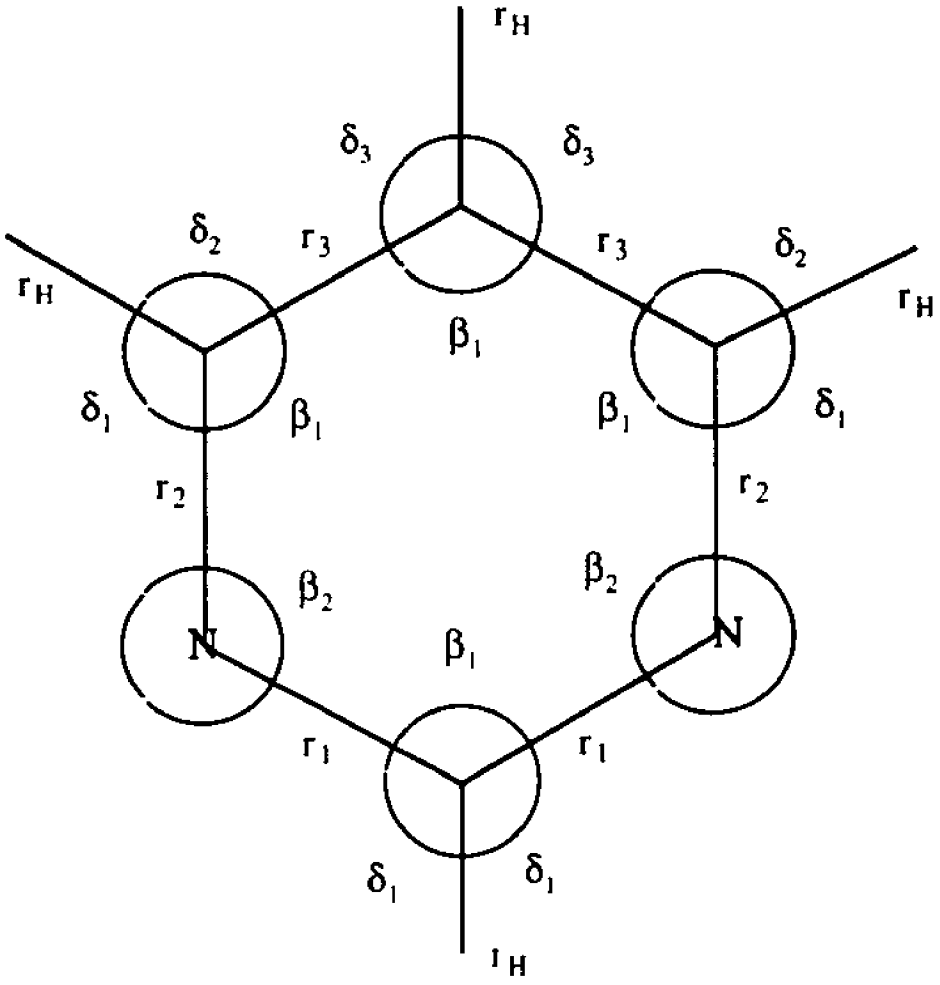
r_H
δ_3
δ_3
δ_2
r_3
r_3
δ_2
r_H
r_H
β_1
δ_1
β_1
β_1
δ_1
r_2
r_2
β_2
β_2
N
β_1
N
r_1
r_1
δ_1
δ_1
r_H

Figure 2.4

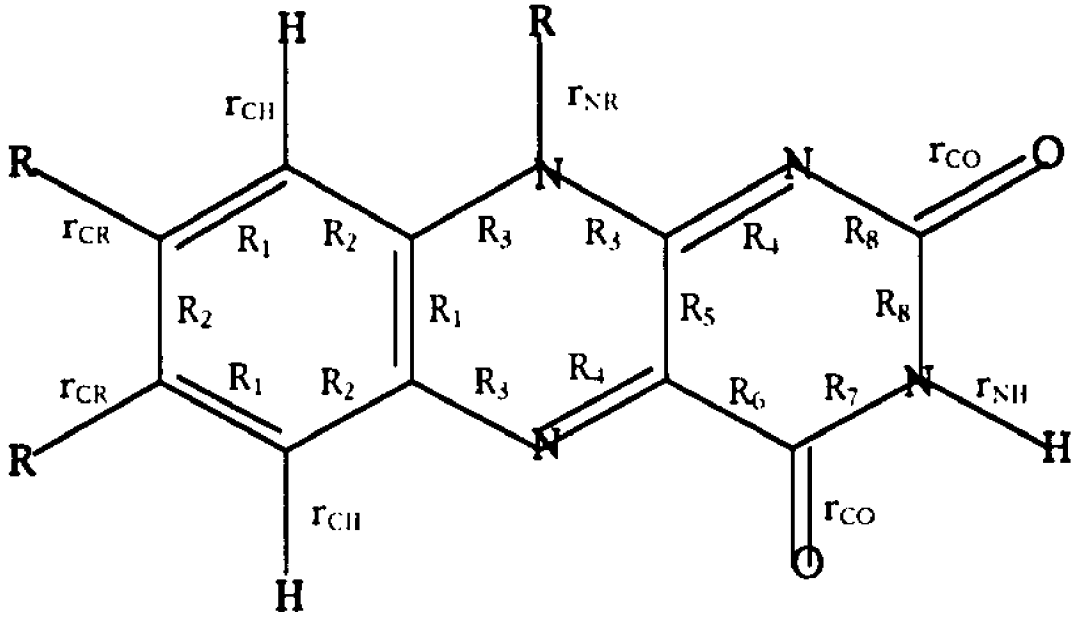
H
R
r_{CH}
r_{NR}
R
r_{CR}
N
N
r_{CO}
O
R_1
R_2
R_3
R_3
R_4
R_8
R_2
R_1
R_5
R_8
r_{CR}
R_1
R_2
R_3
R_4
R_6
R_7
N
r_{NH}
R
N
H
r_{CH}
r_{CO}
H
O

(a)

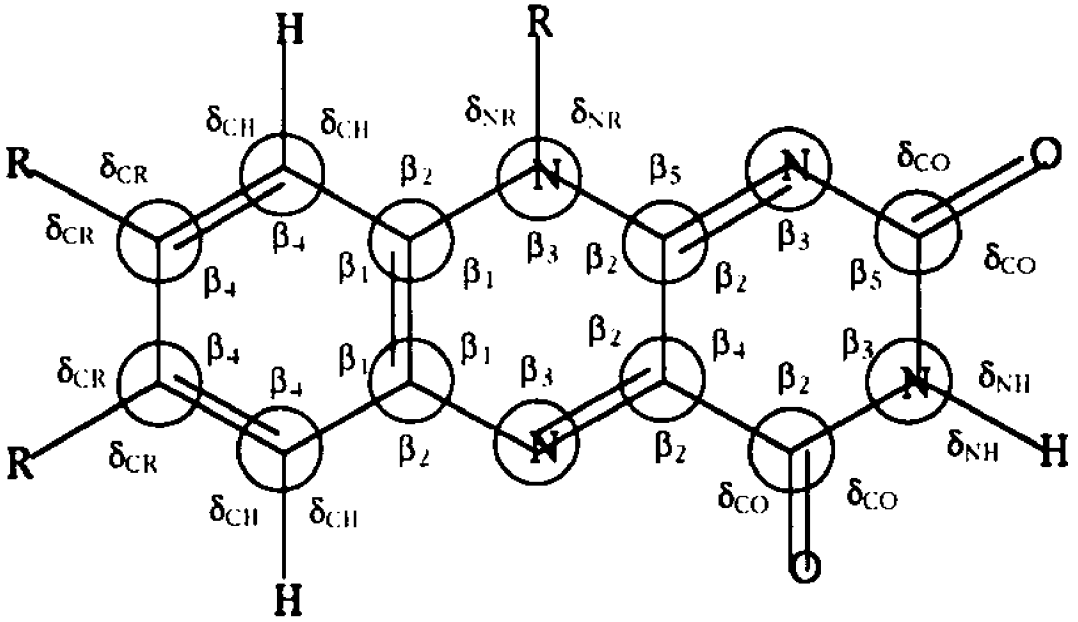
H
R
δ_{CH}
δ_{CH}
δ_{NR}
δ_{NR}
R
δ_{CR}
β_2
N
β_5
N
δ_{CO}
O
δ_{CR}
β_4
β_1
β_1
β_3
β_2
β_2
β_3
β_5
δ_{CO}
β_4
β_2
β_3
δ_{CR}
β_4
β_4
β_1
β_1
β_3
β_2
N
δ_{NH}
R
δ_{CR}
β_2
N
β_2
δ_{NH}
H
δ_{CH}
δ_{CH}
δ_{CO}
δ_{CO}
H
O

(b)

Figure 2.5

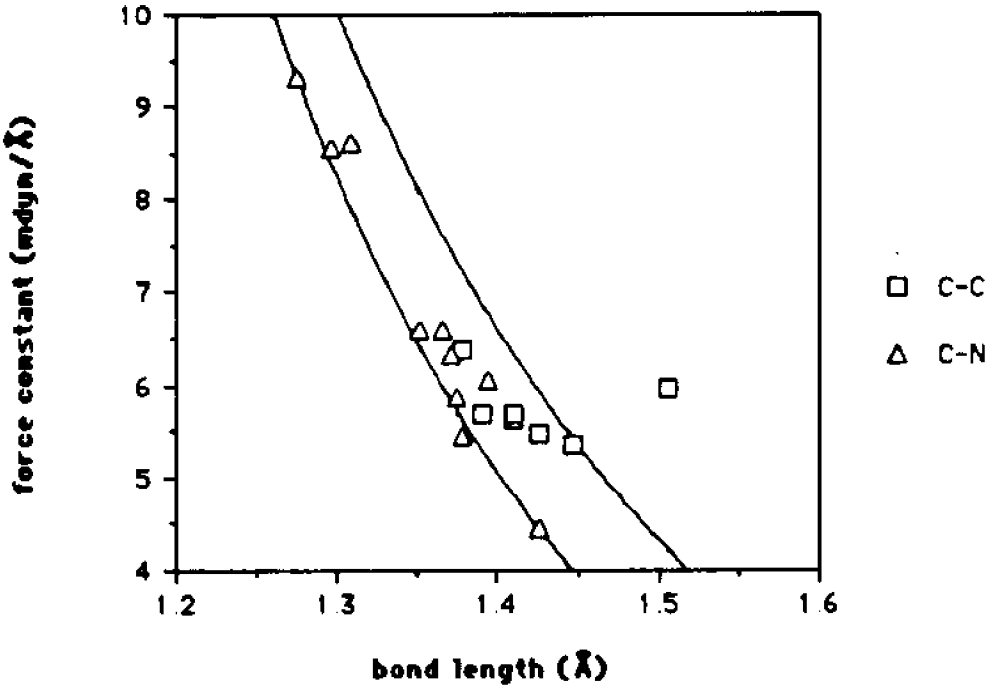
10
9
8
7
6
5
4
1.2
1.3
1.4
1.5
1.6
force constant (mdyn/Å)
bond length (Å)
C-C
C-N

Figure 2.6(a)

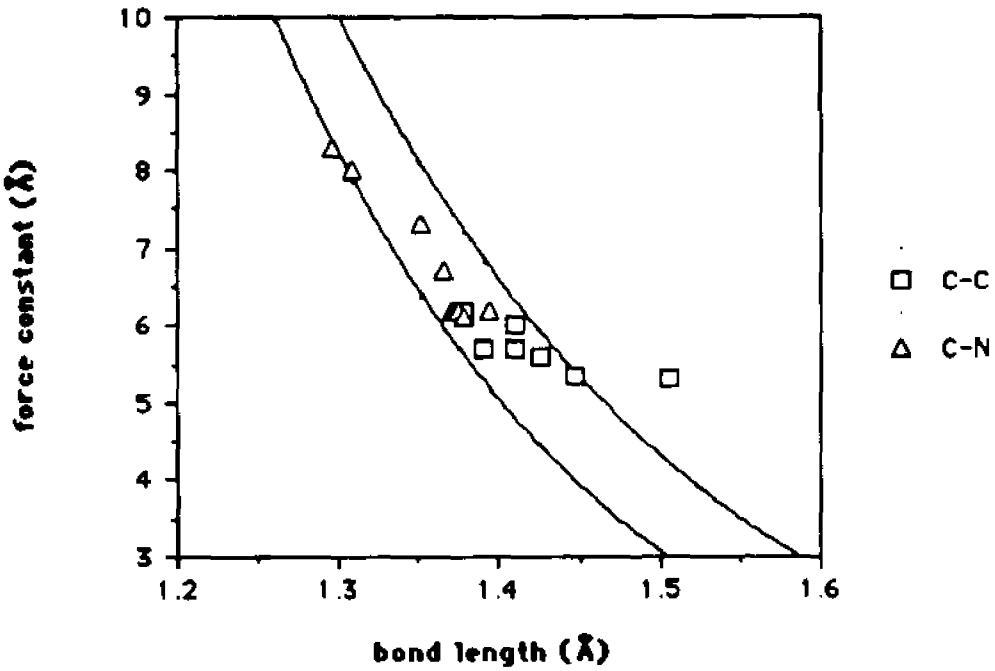

Figure 2.6(b)

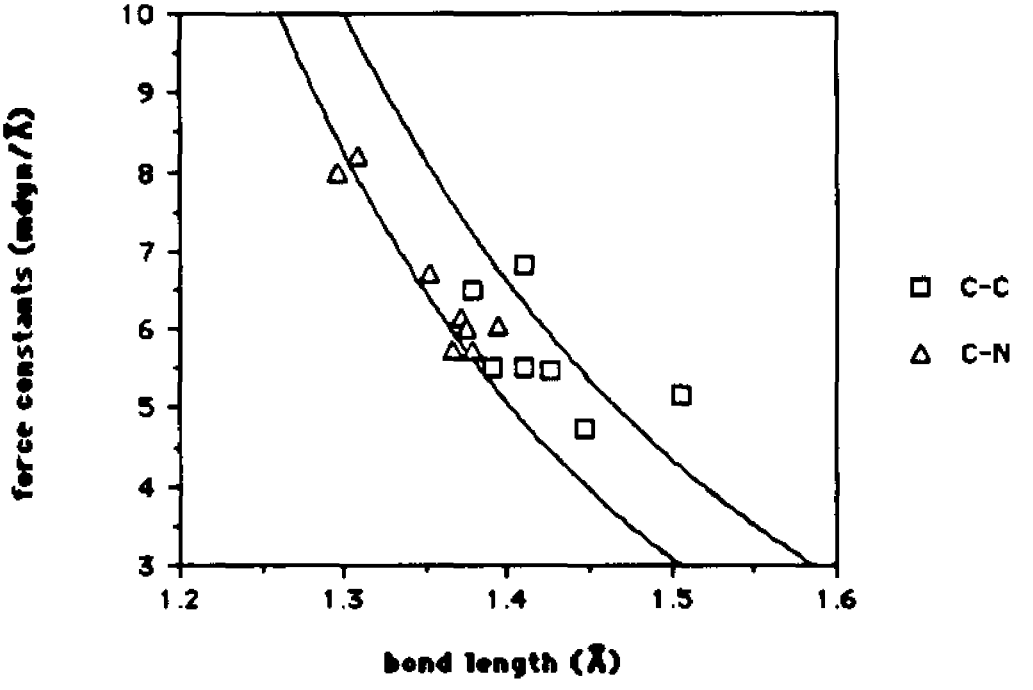
10
9
8
7
6
5
4
3
1.2
1.3
1.4
1.5
1.6
force constants (mdyn/Å)
bond length (Å)
C-C
C-N

Figure 2.6(c)

Chapter III: Normal Mode Calculations of Ammonia and Pyridine Adsorbed on a Silver Electrode Surface

3.1 Introduction

Surface enhanced Raman scattering (SERS) is a powerful technique for studying molecular vibrations and surface chemistry since the normal Raman signals are enhanced by a factor of about 10^4.[1] SERS is also particularly suited for studying molecules of biological interest for various reasons. It has no interference from the medium nor from fluorescence and it requires small sample concentrations (10^{-3} M or less). Also, by choosing an appropriate supporting electrolyte, one can reproduce the natural environment of the molecule under study.

In addition to its technical advantages, SERS holds a special interest because of the enhancement phenomenon.[2] Several mechanisms are believed to take place at the same time; one will dominate over the others depending on the experimental conditions. The two mechanisms thought to contribute the most to the enhancement are the electromagnetic[3] and charge transfer resonance effects.[4]

We set out to use normal coordinate calculations to better understand the molecule-surface interactions. Although the calculations did not help elucidate the enhancement

effect, they did reveal interesting information about interfacial mechanism, namely, charge re-distribution, structural changes and orientation of the molecule on the surface.

Pyridine was chosen because it is one of the best known SERS systems often used as a model compound. This molecule was the one used when the Raman surface enhancement was first observed[5] and it continues to be widely studied. Yet, its orientation on the surface is still controversial. We here address some of these aspects. The other molecule we investigated was ammonia. This molecule was chosen for its simplicity. It requires few parameters, therefore, avoiding the trap of being able to fit anything with enough parameters.

3.2 Procedure

The normal coordinate analysis of the molecules adsorbed on the electrode surface was carried out by comparing the solution normal Raman and the SERS spectra. On inspection, one notices that some frequencies in the SERS spectra are shifted from their normal Raman positions. In these studies, we analyzed the surface-molecule interactions in terms of these frequency shifts.

We proceeded by first calculating the normal modes from the solution spectra. We then perturbed the system with

different modeling steps until we found the results which most closely agreed with the experimental results. The surface was represented by a metal adatom. The modeling steps included the addition of the metal adatom's internal coordinates and their force constants, addition of Urey-Bradley non-bonded interactions between the molecule and the surface atom, changes in the molecule's geometry and variations of the force constants obtained from the solution calculations. The force constants were optimized with the restricted simplex method developed previously.[6]

The surface-molecule interaction was modeled by attaching ammonia and pyridine perpendicularly to the surface. In this arrangement, the molecule forms a chemical bond to the surface through the lone pair electron orbital on the nitrogen. Evidence for this orientation and specific parameters of interaction will be discussed in the following sections. The representation of the surface as an adatom is an approximation. However, results from this laboratory[7] showed that, with this approximation and a two point mass model, they could fit the Ag-N band of many heteroaromatic molecules. Experiments with 2,6-lutidine[8] also support the this model. The methyl groups on a-carbons keep this molecule from interacting in any other way than with an adatom.

3.3 Results and Discussion

3.3.1 *Ammonia*.

In solution, the N-H stretching frequencies shift down from their gas phase values and the H-N-H symmetric deformation shifts up. These shifts are due to hydrogen bonding.[9] On the surface, the N-H stretching and the H-N-H symmetric deformation frequencies shift in the same direction as in solution but further. Information about the surface-ammonia interaction was obtained by reproducing the shifts between the solution and SERS spectra.

For these calculations, the force field was chosen on the basis of fitting the NH_3 and ND_3 gaseous frequencies with the least number of parameters. The force constants obtained from the gaseous calculations were then modified to fit previous results from this lab[10] for solution and SERS frequencies. Table 3.1 shows the observed and calculated results. Table 3.2 shows the force constants obtained by the restricted simplex method from the gas, solution and SERS calculations.

The model for the SERS calculations was set-up by attaching a neutral silver atom to the nitrogen on the ammonia. This is a reasonable model since ammonia is a Lewis base and donates charge from its nitrogen lone pair orbital. This is also the way that ammonia complexes with a silver ion.[11] Several quantum mechanical studies have been done on surface-ammonia models.[12] INDO/S calculations by Rodriguez and

Campbell showed that the HOMO of the free ammonia—mainly nitrogen lone pair—is the orbital most stabilized upon bonding to a zinc oxide surface.[13] Bagus and Hermann showed that, in addition to the charge donation, there is a strong dipole-dipole interaction.[14] From normal mode calculations, we can relate the strength of a bond to its stretching force constant, but we can infer indirectly about the electrostatic effects.

The interaction with the surface was represented by a Ag-N stretching coordinate and a Ag-N-H bending coordinate. The Ag-N and Ag-N-H force constants were determined by adjusting the values to fit the 325 and 665 cm^{-1} bands respectively. It comes as no surprise that these frequencies are slightly lower than their counterparts in the silver-amine complex. One expects the Ag-N bond on the surface to be weaker than on a silver ion because of the smaller charge on the adatom.

The most notable difference between the solution and the SERS spectra of ammonia is the opposite shifts of the hydrogen deformation frequencies. While the symmetric deformation shifts up 48 cm^{-1} to 1174 cm^{-1}, the antisymmetric shifts down by 6 cm^{-1} to 1624 cm^{-1}. The Ag-N-H parameter increased both the symmetric and anti-symmetric hydrogen deformations (the symmetric more dramatically than the anti-symmetric). The Ag-N parameter increased the symmetric deformation by 9 cm^{-1} and left the antisymmetric deformation virtually intact. The best way to reproduce the desired

shifts was by increasing the H-N-H angle and decreasing the H-N-H bending force constant. The angle used in the gaseous and solution calculations was that of the free ammonia, 107.3°. At each 1° increment in the H-N-H angle, the normal modes were calculated with h-deformation force constant values above and below the solution value. In the 112.3° region, the normal modes were calculated at increments of 0.3°. The angle which yielded the best results was 112.3°. The H-N-H force constant change is shown in table 3.2. Other modifications besides the ones mentioned above were tried but didn't reproduce the observed shifts. These included Urey-Bradley non-bonded interactions between the adatom and the hydrogen, decrease of the H-N-H bond angle, adding silver atoms to the adatom.

Figure 3.1 shows the changes on the hydrogen deformations with respect to modeling steps. The lowering of the N-H stretching force constant was due to the decrease of the frequencies in the 3000 cm^{-1} region. This decrease may be correlated to the decrease of these same frequencies when comparing the gaseous and liquid spectra(table 3.2). The larger error of the calculated gaseous frequencies are due to optimizing both the NH_3 and the ND_3 at the same time.

The increase in the H-N-H angle and the decrease in the hydrogen deformation are directly related to one another. Empirical formulas show that the wider the bond angle, the lower its force constant.[15] On bonding to the surface, the lone pair electron orbital on the nitrogen becomes more

localized, shows less repulsion of the N-H orbitals and allows the hydrogen angles to expand. Gaussian calculations at the STO-3G level showed that the H-N-H angle increased 2° when ammonia was bonded to a neutral silver atom. Although this level does not yield the best results for ammonia, it is practical for calculations with silver atoms. It is also adequate for obtaining relative changes

The sensitivity of the calculations to the geometrical parameters comes as a consequence of the increase accuracy provided by the restricted simplex. In order to test this sensitivity we applied the simplex method to the methyl halides. The optimum H-C-H angle was estimated by running the simplex with variations of one degree steps. The results thus obtained differed from the experimental values by less than 1.5°. It should be noted that H-C-H angles in the methyl halides are larger than tetrahedral as in the Ag-NH_3 model. Pauling attributed this phenomenon to the size of the atoms and the differences between the C-H and C-X bond length.[16]

3.3.2 *Pyridine.*

The orientation of pyridine on the surface has been the object of several studies.[17,18] Arguments in favor of a flat orientation are based on intensity changes of the bands according to their symmetries. However, this method has fairly large uncertainties and its conclusions should be accepted with caution. Dudde and Koch showed from photoemission spectra that pyridine binds edge-on to Ag(111)

and Ag polycrystalline substrates.[19] Although the interfacial mechanism at these surfaces may not correlate directly with those of SERS, these results represent the closest experimental evidence for the orientation of pyridine on a Ag surface.

Susuki and Orville-Thomas presented some results that can be viewed as additional evidence for an edge-on interaction.[20] These authors noticed that the 605 cm^{-1} band shifts up 10 to 30 cm^{-1} when pyridine complexes with 8 metal ions. The shifts of the 605 cm^{-1} were matched by adjusting the M-N stretching force constant. In this manner, these authors reproduced the M-N bands of all the complexes. The 605 cm^{-1} band behaves similarly in the SERS spectra. Its shift can also be reproduced with the addition of Ag-N stretching force constant. We set-up the model for the normal mode calculations as an edge-on bonding of pyridine to the surface through the nitrogen. The physical basis of our procedure and the final results should then provide another way to deduce pyridine's orientation on the surface.

As with ammonia, the mass of an adatom was used to represent the point of attachment. The force field used in these calculations was transferred from Susuki's data.[21] This author fitted accurately 112 frequencies of pyridine and 7 isotopomers. Susuki's number of parameters was reduced setting the C_2-C_3 stretch equal to the C_3-C_4 stretch, the C-N-C bending equal to the C-C-C bending and all the non-bonded hydrogen interactions equal to each other. With these

reductions, the number of parameters was less than the number of observed SERS frequencies. Figure 3.2 presents the types of force constants used. The modified force field was refined by first fitting the frequencies of pyridine and 4 isotopomers with a restricted simplex. The resulting force constants were then optimized by fitting the normal Raman solution spectrum of pyridine only. The uncertainty is expected to increase when optimizing with only one species since the force constants are not being checked by the isotopomers frequencies. The procedure described above was followed in order to reduce this uncertainty. The restrictions on the simplex insured that the proper assignments were obeyed. The final atomic displacement vectors agreed with those of Susuki.

Most bands on the SERS spectrum have been assigned.[16,17] Only the assignments of the 239 cm^{-1} and 1026 cm^{-1} bands are still questionable. Several researchers claim that the 239 cm^{-1} band is the Ag-Cl stretch which is known to occur in this region.[22,23,24] However, earlier work from this lab[7] demonstrated that spectra of several heteroaromatics taken in Cl^- free solutions still showed a band around 239 cm^{-1}. This band must, therefore, have a component other than the Ag-Cl stretch. The most likely component is a Ag-N stretch since several metal-pyridine complexes also show a M-N band nearby. It is possible, however, that the Ag-N and Ag-Cl frequencies coincide when Cl^- is present. The 239 cm^{-1} band is broad and studies for its resolution have not been successful.

The 1026 cm^{-1} band shows up prominently at a 0.0 V electrode potential and decreases in intensity at more negative potentials. Fleishman *et al.*[5] attributed this band to an interaction between water molecules, pyridine and the surface. However, our normal mode calculations show that a decrease in the N..H non-bonded interaction causes the 1071 cm^{-1} solution band to drop 23 cm^{-1}. The decrease in the N..H non-bonded interaction is expected from an edge-on interaction with the surface through the nitrogen. From inspection, Creigthon assigned two different modes to the 1071 cm^{-1} solution band. From our calculation, we assign the 1071 cm^{-1} mode with a_1 symmetry to the SERS 1026 cm^{-1} band. This is a reasonable assignment since the corresponding mode in benzene shifts down 12 cm^{-1} upon substitution.[25] In mono-substituted benzene, this mode is observed at 1024 cm^{-1}.

To fit the 239 cm^{-1} band, we used a value of 1.5 mdyne/Å for the Ag-N stretch.[7] This value produced a frequency of 212 cm^{-1}. A Ag..Cα non-bonded interaction of 0.2 mdyne/Å increased the frequency to 237 cm^{-1}. The force constant ratios between the Ag-N stretching and the Ag..Cα non-bonded interaction correlate with Rodriguez' MO calculations.[26] This author's INDO/S calculations showed that, for an edge-on model, the nitrogen donates charge to the surface from its lone pair orbital. The whole interaction is 80 to 90% through the nitrogen and the rest through the a carbon and the hydrogen on the a carbon. Ag..H non-bonded parameters did not have much of an effect in our calculations and, hence, were left

out. Fitting the 239 cm^{-1} band with the Ag-N stretch and the Ag..C_α non-bonded interaction force constants produced too large a shift in the 618 cm^{-1} frequency. In order to obtain a better match for this frequency, the C-N-C force constant was lowered. The reason for this lowering will be discussed ahead.

Lowering the N..H non-bonded interaction force constant did not reproduce all of the drop of the 1071 cm^{-1} band. A restricted simplex optimization was required to produce a larger drop. For this optimization, we used the frequencies from the SERS spectrum taken at a -0.2 V potential.[16] The decrease in the N..H non-bonded interaction also produced a drop in the 1355 cm^{-1} frequency. However, this frequency has not been observed in SERS and did not figure in the analysis.

Reproducing the large shift in the 1071 cm^{-1} band placed a large strain on the force field. To relieve the strain during the simplex optimization, several force constants were allowed to vary separately from the force constants they were set equal to when reducing Susuki's number of parameters. The C-N-C bending varied separately from the C-C-C bending, the N..H non-bonding interaction from the C..H non-bonded interaction, and the C..H non-bonding interactions of the C_2-C_3 bond from those on the C_3-C_4 bond. After these changes, the total number of optimized parameters was the same as the number of SERS frequencies being fitted. The 239 cm^{-1} frequency was not included in the optimization. Its low relative value produced large percentage errors and the

simplex weighted it heavily during the optimization. Its calculated value was discussed earlier. Table 3.3 shows the observed and calculated frequency shifts before and after the optimization. The calculated value of the Ag-N band had an error of 2.22 % from the observed value. The average error on the rest of the frequencies was 0.33 %. As expected, the largest error was on 1025 cm^{-1} band, 1.00 %.

Table 3.4 shows the force constants for the solution and SERS calculations. The ring stretch force constants with the largest change was the $K(N_1-C_2)$. This result may be correlated to bond order changes from INDO/S calculations. These calculations show that the decrease of the N_1-C_2 bond order is the largest change in bond order that occurs when pyridine binds to Cu and Zn oxide surfaces.[13,26] The decrease is due to the charge donation from the nitrogen to the surface.

3.4 Conclusion

From the fit of the observed frequencies and their shifts along the physical basis of the procedure followed we conclude that pyridine interacts edge-on with the surface at potentials more positive -0.2 V. Correlation with bond order changes from the INDO/S calculations also supports an edge-on interaction.

Creighton attributed the drop in intensity of the 1026 cm^{-1} band at -0.5 V to a change in the orientation of pyridine

on the surface from edge-on to flat.[17] Since the 1026 cm^{-1} band is absent at this potential, the normal mode calculations do not contradict Creighton's conclusion. However, the SERS of benzene, which is most likely flat, shows that the out-of-plane hydrogen deformations shift up 15 cm^{-1} or more and the out-of-plane ring deformations shift 7 cm^{-1} down.[27] The shifts observed in the out-of-plane modes of pyridine on the surface are not consistent with those of benzene. The out-of-plane hydrogen deformations shift down 6 cm^{-1} or less and the out-of-plane carbon deformations shift up about 3 cm^{-1}. Calculations of the out-of-plane modes with an edge-on model reproduce the observed shifts on the surface. However, those shifts are small in comparison to the error in the calculation.

Moskovits[28] obtained better fits for the Ag-N bands in heteroaromatic spectra than the adatom model proposed by our group by attaching additional silver atoms to the adatom to simulate a metal cluster. However, the normal mode calculation showed that the additional silver atoms affected only the Ag-N band. Consequent adjustment of the Ag-N force constant to fit the Ag-N band had little effect on the other bands. Changes in the mass of the adatom had the same effect as adding additional silver atoms.

There is not much ambiguity about the orientation of ammonia on the surface. From the calculations, we conclude that the H-N-H angle increases upon adsorption.

Table 3.1. Observed and calculated frequencies (in cm^{-1}) of gaseous, solution and SERS spectra of ammonia.*

Gaseous*		Solution Raman†		SERS†		
Obs. freq.	Calc. freq.	Obs. freq.	Calc. freq.	Obs. freq.	Calc. freq.	Assig.‡
3414	3447	3405	3405	3325	3345	υ_a(N-H)
3337	3360	3248	3291	3211	3211	υ_s(N-H)
1628	1641	1630	1630	1624	1623	δ_a(HNH)
950	967	1126	1126	1174	1170	δ_s(HNH)
				674	674	δ_a(AgNH)
				325	325	υ(AgN)

* From ref. (29)

† From ref. (10)

‡ υ: stretch, δ: bend, a: antisymmetric, s: symmetric.

Table 3.2. Force constants in mdyne/Å of gaseous, solution and SERS NH_3 calculations.

Force constant*	Gaseous	Solution Raman	SERS
K(N-H)	6.4355	6.2790	6.0290
H(H-N-H)	0.6340	0.6258	0.5708
f_{s-b}	0.3713	0.1623	0.16230
K(Ag-N)			0.9300
H(AgNH)			0.27500

* K: stretching, H: bending, f_{s-b}: interaction between hydrogen stretching and bending.

Table 3.3. Comparison for pyridine of observed and calculated frequency shifts (in cm^{-1}) between normal Raman and SERS spectra before and after optimization.

Normal Raman frequencies	Observed shift for SERS	Initial calculated shifts	Optimized calculated shifts
1593	+2	+5	+4
1576	-5	-8	-8
1487	+2	+7	+3
1444	0	+2	+7
1232	+6	+6	-2
1220	-6	-12	-3
1153	0	+2	-1
1071	-3	+10	+1
1071	-45	-23	-35
1036	0	+13	-3
1002	+6	+4	+3
654	-3	+1	-2
618	+5	+18	+9

Table 3.4. Force constants results for pyridine in mdyne/Å from normal mode calculations of solution and SERS spectra.

Force constant*	Solution	SERS
$K(N_1C_2)$	5.8948	5.3131
$K(C_2C_3)$	4.6204	5.0905
$K(C_3C_4)$	4.6204	4.6918
H(NCH)	0.3370	0.2233
H(CCH)	0.2904	0.3161
H(NCC)	0.9091	1.0306
H(CCC)	0.6856	0.5513
H(CNC)	0.6856	0.2395
ρ	0.4335	0.4591
F(N..H)	0.5087	0.4169
$F(C_2..H_3,\ C_3..H_2)$	0.5087	0.4168
$F(C_3..H_4,\ C_4..H_3)$	0.5087	0.4207
F(C..C, N..C)	0.5721	0.5794
K(Ag-N)		1.5000
$F(Ag..C_2)$		0.2000

* K: stretching, H: bending, F: non-bonded interaction, ρ aromatic interaction.

Figure Captions

Figure 3.1. Calculated frequency differences between modeling steps of the symmetric and anti-symmetric hydrogen deformation modes: 1) normal Raman solution frequencies, 2) addition of Ag-N stretch, 3) addition of Ag-N-H bending, 4) increase of the H-N-H angle from 107.3° to 112.3°, 5) decrease of the H-N-H bending, 6) decrease of the N-H stretch. SERS frequencies on the right of the graph.

Figure 3.2. Internal coordinates of pyridine used in this work. r: stretches, d: hydrogen deformation, b: ring deformations.

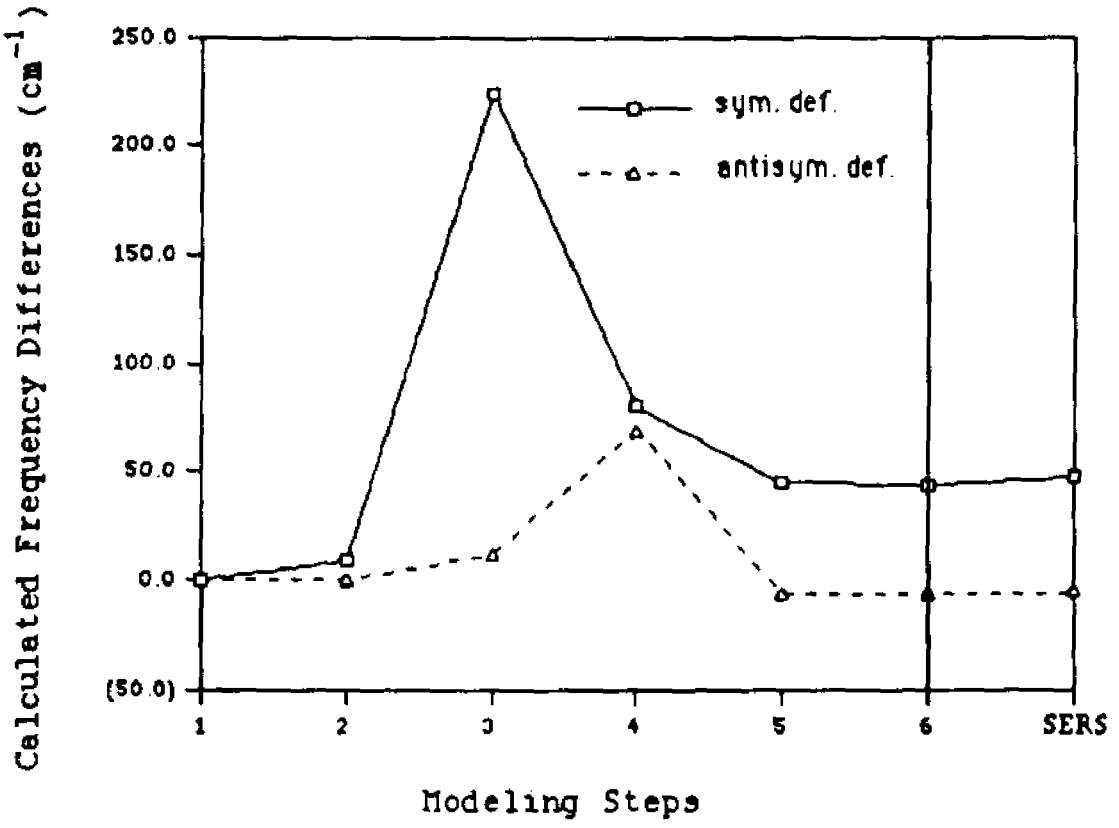
Calculated Frequency Differences (cm^{-1})
250.0
200.0
150.0
100.0
50.0
0.0
(50.0)
sym. def.
antisym. def.
1
2
3
4
5
6
SERS
Modeling Steps

Figure 3.1

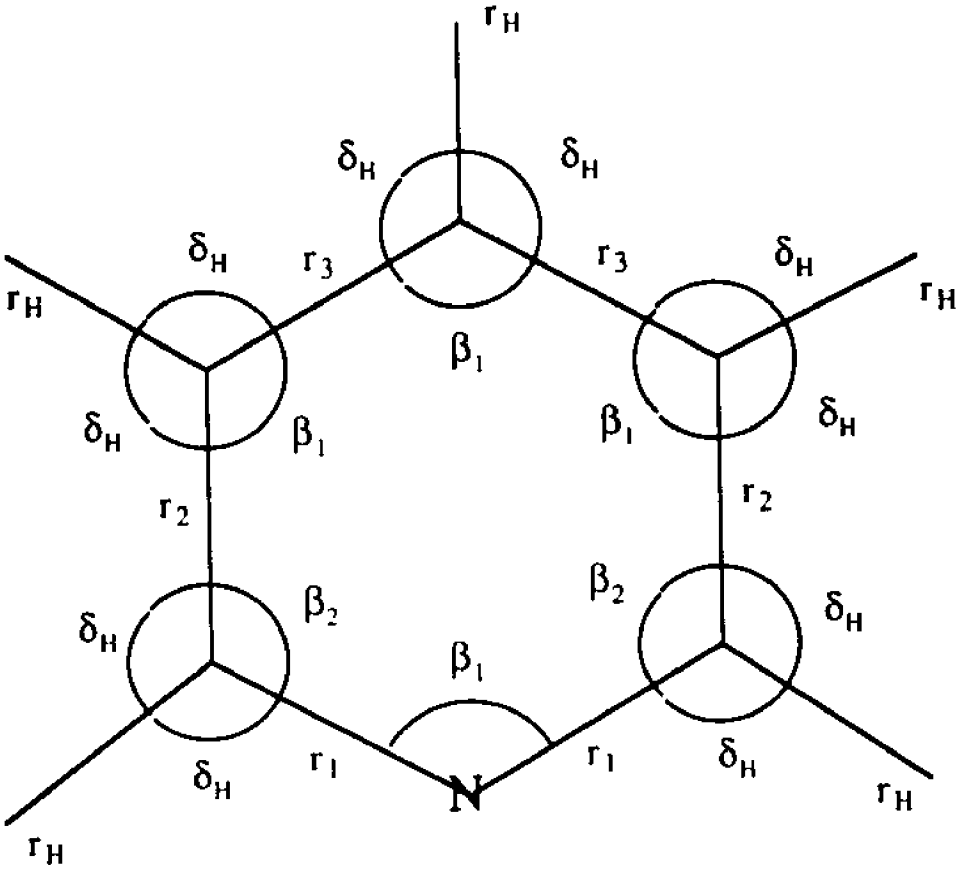
r_H
δ_H
δ_H
δ_H
r_3
r_3
δ_H
r_H
r_H
β_1
δ_H
β_1
β_1
δ_H
r_2
r_2
β_2
β_2
δ_H
δ_H
β_1
δ_H
r_1
r_1
δ_H
r_H
N
r_H

Figure 3.2

Chapter IV: Analysis of the SERS Spectra of Adenine and NAD^+

4.1 Introduction

NAD^+ and its reduced form, NADH, hold a special interest for biologists, biochemists and biophysicists because these coenzymes play a major role in numerous oxidation-reduction processes in our body. Surface enhanced Raman scattering spectroscopy (SERS) can yield information about these molecules interfacial behavior, i.e. bonding to metal surfaces, oxidation-reduction potentials, conformation analysis, charge distribution, etc. SERS spectra of NAD^+ on colloidal silver had been obtained and analyzed previously.[1-3] In the present study, the SERS spectra of NAD^+ on an electrode surface is analyzed. The spectra were taken under various conditions of electrode potential, pre-treatment, and NAD^+ and electrolyte concentration.

To help interpret the SERS spectra of NAD^+ on colloid particles and on the electrode surface, normal coordinate calculations of adenine were carried out. Two of this molecule's bands dominate the NAD^+ spectra. The way these two bands behave can reveal information about the NAD^+'s interaction with surfaces. This chapter presents the

experimental and calculation results and the conclusions drawn from them.

4.2 Experimental

NAD^+ was purchased from Sigma Chemical Co. Two types of supporting electrolyte solutions were used: a phosphate buffer at two different concentrations, 0.15 M and 0.05 M and a 0.1 M KCl solution. The phosphate buffer was made from equal amounts of Na_2HPO_4 and KH_2PO_4. The Na_2HPO_4, KH_2PO_4 and KCl were reagent grade. All aqueous solutions were made with deionized distilled water and deareated by nitrogen bubbling for 20 minutes.

The pH was adjusted by titrating the solutions with reagent grade concentrated H_3PO_4 or HCl. Spectra were taken at pH's 7.0, 6.6, 5.6, 4.6 and 3.5 when titrating with HCl and 7.0, 4.8 and 3.0 when titrating with H_3PO_4. pH measurements were done with a Model 720 Orion Research Digital Ionalyzer.

The sample cell consisted of a silver working electrode, a Pt counter electrode and a saturated calomel electrode (SCE) as reference. The electrode was pre-treated in two ways with an oxidation-reduction cycle (ORC) to roughen its surface: a) *in situ* with the phosphate buffer or the KCl solution, b) *ex situ* in a KCl solution. The applied potential step for the ORC with the phosphate solution was from 0.0 V

to +0.5 V and -0.2 V to +0.2 V in the KCl solution. For all solutions, spectra were taken as a function the number of ORC's.

As an excitation source, a 488 nm line from a Spectra-Physics Model 164 Ar^+ Laser was used. The spectra were obtained with a Spex Model 1401 double monochromator with a photon counting detector.

4.3 Normal Modes of Adenine

Normal mode calculations of the in-plane vibrations of adenine (figure 4.1) were carried out since this molecule's bands are the most intense in the NAD^+ SERS spectra. The initial force constants were taken from Majoube's Urey-Bradley force field.[4] This force field was reduced using the transference approximation in order to obtain an under-determined system. The experimental frequencies of adenine and the deuterated species were also taken from Majoube. The $-^{15}N1,3$ and $-^{13}C8$ frequencies were obtained from Hirakawa *et al.*[5]. All observed Raman frequencies were used to allow a direct comparison with the SERS frequencies. IR values were used for those modes that were not observed in the Raman spectra. The geometrical parameters were obtained from Nowack *et al.*[6] The force constants were optimized with the simplex optimization described in chapter II. Different sets of restrictions were tried. Each result was evaluated on the

basis of the frequency and isotopic shift matches. Table 4.1 shows the results of adenine and the two deuterated species. Table 4.2 shows the observed and calculated isotopic shifts of the $-^{15}N1,3$ and $-^{13}C8$ species.

Three models describing the possible forms of attachment of adenine to the Ag surface were studied. These are shown in figure 4.2. Only models representing a perpendicular interactions were studied since they affect the in-plane vibrations the most. Although a parallel interaction is not ruled out, the lone pair electrons in the adenine nitrogen provide the most likely binding sites. The Ag surface was represented by a silver ad-atom.[7] The surface-molecule interactions included the Ag-N stretching and the Ag..C_α non-bonded force constants. The surface interaction force constant values were transferred directly from pyridine the calculation from chapter III. The SERS spectra on silver colloid was obtained from Siiman *et al.*

Calculation of the N7-H tautomer and the imino conformation were also carried out. The N7-H calculation was done by adding the surface interactions parameters, exchanging the N_7C_8 and C_8N_9 stretches and adjusting the N7-H bending and non-bonded interaction to fit the 1390 cm^{-1} band. While the N_9 and N_7 are equivalent, the hydrogen bonded to these atoms move in different environments. Their bending force constants should therefore have different values. The imino calculation was done by shifting one of the amine hydrogens to N1 and shifting the πbond from N_1-C_6 to C_6-N_{10}.

4.4 Results and Discussion

4.4.1 *SERS Spectra of Adenine.*

The models on figure 4.2 were evaluated on how well they reproduced the up-shifts in the SERS spectra of the 1330 and 722 cm^{-1} bands when comparing to the solution spectra and on accounting for the 1390 cm^{-1} band. The up-shift of the 722 cm^{-1} is the most conspicuous difference between the SERS and solution spectra. This band is strong and sharp and its shift can be measured unambiguously. The 1330 cm^{-1} band is also strong though somewhat wider. The 1390 cm^{-1} band appears in the SERS spectra on silver colloid as a weak shoulder and only at concentrations of 0.10 mM. In the solution spectra, it is a moderate size band.[8]

One possible way that adenine can bind to the surface is through N1 (figure 4.2a) since this nitrogen has the largest charge density of all the nitrogen in the molecule.[9] However, this form of attachment is ruled out because it does not reproduce the up-shift of the 722 cm^{-1} band. Figure 4.2b represents an interaction of the imino form of adenine with the surface. This complex was proposed by Siiman *et al.* as formed during a reaction of NAD^+ with Tollens' reagent. The model, however, failed to reproduce the up-shifts of both 722 and 1330 cm^{-1} bands. Only an attachment through N_3, figure 4.2c, accounted for the shifts of these bands. The Ag-N_3 model also accounted for the 1390 cm^{-1} band by allowing tautomerization to occur. The N7 tautomer (figure 4.1) is

relatively stable since it is the dominant tautomer in crystal purine.[9] The N7-H tautomer calculation showed a N_7-H deformation frequency in this region.

Lord and Thomas[10] observed a band in the adenine spectrum at 1430 cm^{-1} that probably corresponds to the 1390 cm^{-1} of Yue *et al.* spectrum.[8] The 40 cm^{-1} differences between the two bands may be attributed to different pH conditions. The spectrum of Yue *et al.* was taken at pH 7.0 and Lord and Thomas' at 0.5. Upon deuteration, the 1430 cm^{-1} band in the latter spectrum shifted down 32 cm^{-1}. The calculated N_7-H deformation band in this region shifted down 39 cm^{-1} upon deuteration.

Protonation at the N1 position had the same effects on the 1390 cm^{-1} band described above for the N7 tautomer. A N_1-H model is supported by the fact that N_9-substituted adenines also show a band in this region.[8] N_1 is a favorable protonation site because of its large charge density; but, protonation occurs at a pH of 4.2 and the SERS spectrum was taken at pH 6.0. N_1 is also protonated in adenine's imino conformation, figure 4.2b. However, this model was discarded as a possible attachment model for reasons already discussed.

Table 4.3 shows the calculated frequencies of N9 and N7 tautomers and compares them with the experimental frequencies from the crystal, solution and SERS spectra. For the most part, the frequencies of both tautomers were the same in value and composition. Normal modes with a 10 % contribution from the N_9-H or N_7-H deformations were considered as

different bands. Only two bands in the SERS spectra remained unaccounted for. The rest were assigned from the calculated values and from out-of-plane data.[4,11] The calculation was also consistent with what is observed in the solution spectra. The less certain assignments are discussed below.

The surface interaction parameters at the N3 bonding site caused the desired up shift of the 722 cm^{-1} band. They also caused the 898 cm^{-1} band to shift up 38 cm^{-1}. From inspection, one would correlate 898 cm^{-1} in the crystal spectra with 895 cm^{-1} of SERS and 976 cm^{-1} to 990 cm^{-1} in the solution spectra. However, from the calculations, we assign the 898 cm^{-1} band to 976 cm^{-1} and the 990 cm^{-1} band to the out-of-plane mode reported by Dhaouadi *et al.* at 943 cm^{-1}.[10] The SERS 895 cm^{-1} band along with the solution 872 cm^{-1} band is then assigned to the 870 cm^{-1} out-of-plane mode. The surface interactions also produce a band around 224 cm^{-1}. This could be the Ag-N band observed in other heteroaromatics in that region.[7] It could also be the 240 cm^{-1} out-of-plane mode.

The 1071 and 605 cm^{-1} frequencies have the largest difference between the observed and calculated values, 6.2 % and 6.4 % respectively. The 605 cm^{-1} fit is still acceptable since the lower frequencies tend to have larger relative errors. Nevertheless, this band could be the 624 cm^{-1} out-of-plane mode in Dhaouadi *et al.* spectrum. The 1071 cm^{-1} band appears in the solution and SERS spectra but not in the crystal spectrum. Imidazole has a hydrogen deformation mode in the 1070 cm^{-1} region while crystal adenine does not. Hence,

the appearance of this band in solution and on the surface is attributed to tautomerization. It may be assigned to the N7-H tautomer mode at 1138 cm^{-1} with a large hydrogen bending contribution. The large error is due to the rough approximations of the N7-H tautomer calculation.

All frequencies in the SERS spectra are accounted for by the calculations described above except for 488 and 457 cm^{-1}. These two frequencies do not appear in crystal nor solution spectra. They may be ring out-of-plane modes which shift down upon interaction with the surface.

4.4.2 *SERS Spectra of NAD^+.*

The electromagnetic enhancement factor causes the molecular vibrations closest to the surface to have the most intense bands in SERS spectra. In the experiments here presented, the NAD^+ bands that lose the most intensity at low pH are those at 1458, 1162, 1112 and 1031 cm^{-1} (asterisks in figure 4.3a). These bands are associated with the nicotinamide(NMN) part of the molecule (figure 4.4). The NMN bands also lose intensity at a more negative potential (asterisks in figure 4.3b). These results indicate that NMN is close to the surface at neutral pH's and low negative potentials and moves away from the surface as the pH is lowered and the potential becomes more negative.

Adenine's 1330 cm^{-1} and 730 cm^{-1} bands are the most intense in the NAD^+ electrode surface spectra. These bands hardly change as a function of pH and potential indicating

that adenine strongly binds to the surface under various experimental conditions. The SERS shifts of these two bands do not correlate directly with the adenine SERS shifts discussed in the last section. The 1330 cm^{-1} band shifts downward and the 730 cm^{-1} band shifts slightly upward. The normal mode calculation show that the model in figure 4.2b reproduce these changes. The Ag-N_7 and Ag-N_{10} bonds caused a small upward shift to the 730 cm^{-1} band. Decreasing the N1-C6 stretching force constant, as a consequence of the π bond shift from N_1-C_6 to C_6-N_{10}, caused a down shift of the 1330 cm^{-1} band. Assignments of most of the bands in the NAD^+ SERS spectra are shown in table 4.4.

Different from colloid silver experiments, variations in NAD^+ concentration did not cause changes to the electrode surface spectra. Using KCl for pre-treatment or as electrolyte solution made the spectra less sensitive to pH and potential changes. Finally, the number of oxidation-reduction cycles during *in-situ* pre-treatment caused changes in the spectra. However, these changes had low reproducibility.

Relative intensity differences between the adenine and NAD^+ spectra on colloidal silver support the orientations here proposed. In adenine, the 739 cm^{-1} band is the most intense. The largest contribution to this mode is from the N_3-C_4 stretch. In NAD^+, the 1390 cm^{-1} band becomes the most intense band. This band is mostly a N_7-C_8 stretch. The most intense band in the SERS spectra at 0.0 V electrode potential

and pH 7.0 occurs at 1324 cm^{-1}. In this case, the molecules orientation cannot be deduced from the band intensity because this mode has large contributions from both N_3-C_4 and C_5-N_7 stretching. However, its down shift from the NAD^+ solution spectra can only be explained by the imino model. Adenine's 1340 cm^{-1} mode in the colloid silver spectra shifts down in NAD^+ for the same reason. Why the intensities of adenine's 1390 cm^{-1} and 1340 cm^{-1} bands differ between the silver colloid and electrode surfaces is not understood yet. It may have to do with the interaction of the rest of the molecule with the different surfaces.

4.5 Conclusion

Austin and Hester[2] did not observe SERS enhancement of NADH at an alkaline pH. Since the colloidal particles lose their positive charge upon coordination with hydroxide, these authors concluded that the interaction of NAD^+ and NADH was charge dependent and, consequently, through the phosphate groups. However, the normal mode calculations and the intensity changes strongly suggest that NAD^+ bonds to the surface through N_7 and N_{10}. The evidence here presented does not refute Austin and Hester's conclusion about NADH's interaction with the surface. It only contradicts the assumption that NAD^+ and NADH behave the same way. The normal

mode calculation also show that adenine bonds to the surface through N_3.

There is disagreement about the way the NMN ring attaches to the surface. Siiman *et al.* suggested that the NMN alignment on the surface depends on the concentration of the molecule. We found no such dependence. This discordance may be due to the differences between the colloidal silver and silver electrode surfaces. From the pH and potential dependence spectra we conclude that the NMN lies close to the surface at the higher pH's and more positive potentials and moves away from the surface at low pH's and more negative potentials.

We found no conclusive evidence about the behavior of the ribose rings and phosphate group. However, in order for the adenine and NMN to interact with the surface in the manner described above, NAD^+ must spread out through the surface. A molecular model shows that NAD^+ is sufficiently flexible to allow this spreading out.

Table 4.1. Observed and calculated frequencies (in cm^{-1}) of adenine, -N9,10-d_3 and -C_8-d.*

Adenine		-N9,10-d_3		-C_8-d	
Obs. freq.	Calc. freq.	Obs. freq.	Calc. freq.	Obs. freq.	Calc. freq.
3295	3378	3120	3117	3315	3378
3115	3275	3045	3089	3135	3275
3125	3117	2490	2506	-	3089
3038	3089	2381	2365	2800	2789
2790	2789	2160	2048	2335	2292
1675	1670	1610	1624	1674	1670
1612	1635	1568	1581	1612	1635
1597	1580	1514	1526	1595	1579
1510	1526	1466	1479	1499	1525
1482	1495	1450	1439	1478	1481
1462	1468	1424	1382	1463	1466
1418	1426	1372	1365	1405	1415
1370	1378	1333	1331	1365	1370
1331	1348	1305	1301	1322	1344
1307	1311	1250	1239	1305	1308

* Observed frequencies from ref. (4).

Table 4.1. Continued.

Adenine		-N9,10-d_3		-C_8-d	
Obs. freq.	Calc. freq.	Obs. freq.	Calc. freq.	Obs. freq.	Calc. freq.
1248	1244	1230	1225	1235	1217
1235	1208	1178	1177	1173	1173
1164	1168	1100	1100	1123	1129
1126	1129	970	966	1023	1028
1023	1028	933	927	955	957
940	935	888	905	918	928
898	914	853	837	862	879
722	718	706	703	717	715
620	633	602	604	622	630
558	560	560	539	542	551
535	536	525	525	529	535
330	330	302	302	323	327

Table 4.2. Observed and calculated frequencies of adenine and the $^{15}N1,3$ and $^{13}C8$ isotopic species.*

Adenine		$^{15}N1,3$		$^{13}C8$	
Obs. freq.	Calc. freq.	Obs. shift	Calc. shift	Obs. shift	Calc. shift
1675	1670	0	0	0	0
1612	1635	7	4	2	0
1597	1580	6	6	4	1
1510	1526	5	6	3	2
1482	1495	7	1	8	11
1462	1468	2	2	7	2
1418	1426	2	0	10	17
1370	1378	6	5	2	4
1331	1348	17	10	3	0
1307	1311	11	12	2	1

* Observed frequencies from ref. (5).

Table 4.2. Continued.

Adenine		^{15}N1,3		^{13}C8	
obs. freq.	calc. freq.	obs. shift	calc. shift	obs. shift	calc. shift
1248	1244	6	4	4	4
1235	1208	4	11	3	1
1164	1168	3	0	15	12
1126	1129	7	6	4	5
1023	1028	8	8	1	0
940	935	4	2	5	1
898	914	12	15	3	1
722	718	7	7	3	3
620	633	8	10	1	2
558	560	7	3	1	1
535	536	5	4	3	1
330	330	2	0	0	1

Table 4.3. Crystal, solution and SERS spectra of adenine and their assignments.

Cryst.*	Soln.†	SERS‡	N_9-H calc.	N_7-H calc	Assignment
1675			1670	1670	$C_6N_{10}H$ def.
1612			1641	1626	C_3C_4 str.
1597	1596		1583	1593	C_4C_5 str.
	1569				
1520		1538	1530	1530	C_6N_1 str.
	1497		1495		
1482	1485			1484	C_4N_9H def.
1462		1456	1469	1463	C_4N_9H def.
1418	1419	1405	1427		C_8C_9 str.
	1396	1390		1419	
1370	1363	1369	1380	1383	C_6N_1 str.
1331	1330	1340	1352	1341	C_5N_7 str.
1307	1309	1324	1314	1320	N_1C_2 str.
		1267			
1248	1249		1245	1244	N_7C_8 str.
1235		1213	1211	1210	C_2N_3 str.
1164	1148	1138	1170		C_8N_9 str

* From ref. (4).

† From ref. (8).

‡ From ref. (1).

Table 4.3. Continued.

Crystal	Soln.	SERS	N_9-H calc.	N_7-H calc	Assignment
1126	1121		1141	1140	C_8C_9 str.
	1079	1071		1138	
1023		1029	1029	1027	$C_6N_{10}H$ def
	990				943 o/p
940	948	931	931	924	$C_5N_7C_8$ def.
898		976	952	953	$C_2N_3C_4$ def.
	872	895			870 o/p
		833			840,850 o/p
		810			797 o/p
		790			771 o/p
722	722	739	735	739	N_3C_4 str.
		690			680 o/p
		643			640, 655 o/p
620	622	633	639	638	C_5C_6 str.
558		605	566	572	$N_1C_2N_3$ def.
535	539	562	555	550	$C_2N_3C_4$ def.
		488			
		457			
330		330	336	334	$N_1C_2N_3$ def.
	302				315,310 o/p
		224	211	208	240,238

Table 4.4. Frequencies (in cm^{-1}) and their assignments of NAD^+ at various electrode potentials and pH's.

7.0 pH, 0.0 V	7.0 pH, -0.5 V	4.8 pH, 0.0 V	3.8 pH, 0.0 V	Assignments
1644	1644	1644		
1606		1606	1600	adenine
1578	1578	1578		adenine - ribose
1516	1516	1516	1516	adenine - ribose
1458	1458	1458	1458	NMN - ribose
1438				
1378	1398	1398	1398	adenine - ribose
1326	1326	1326	1326	adenine
	1248	1248	1248	adenine
	1184			NMN - ribose
1162	1162			
1112	1112	1112		ribose - phosphate
1074				phosphate
1030	1030	1038	1030	NMN

Table 4.4. Continue.

7.0 pH, 0.0 V	7.0 pH, -0.5 V	4.8 pH, 0.0 V	3.8 pH, 0.0 V	Assignments
988	988	998		NMN
958	958	958	958	NMN - ribose
		909		adenine o/p
			800	adenine o/p
774				adenine o/p
734	734	734	734	adenine o/p
688	682	688		adenine o/p
648	652			adenine o/p
		622	622	
564	562	564		ribose - phosphate
542		542		adenine
328	328	328		adenine - phosphate
232	232	232		

Figure Captions

Figure 4.1 Adenine: a) N9 tautomer, b)N7 tautomer.

Figure 4.2 Possible binding models of adenine on a silver surface.

Figure 4.3(a) pH dependence spectra of NAD^+; top: pH=3.0, bottom: 7.0.

Figure 4.3(b) Potential dependence spectra of NAD^+; top: -0.05 V, bottom: 0.0V

Figure 4.4 Nicotinamide.

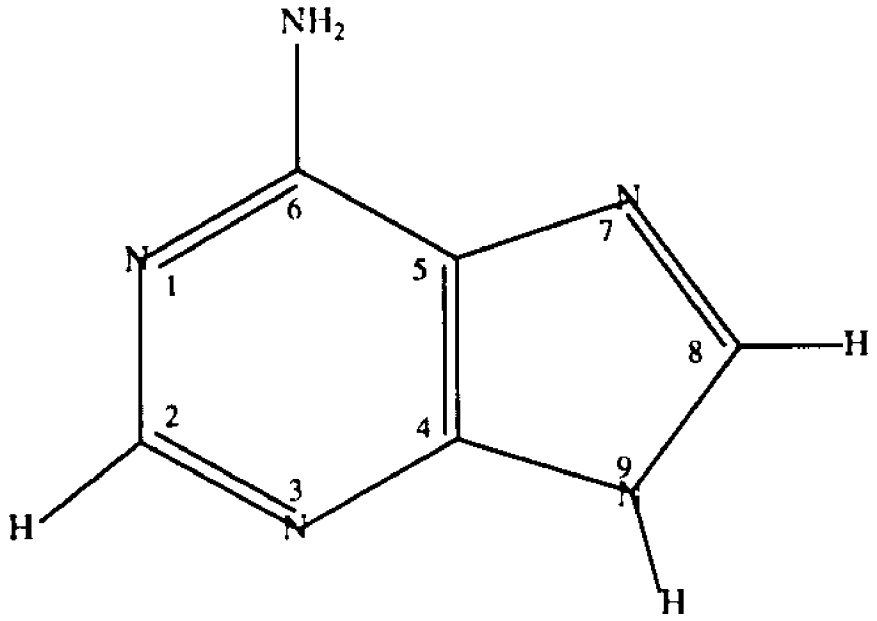

(a)

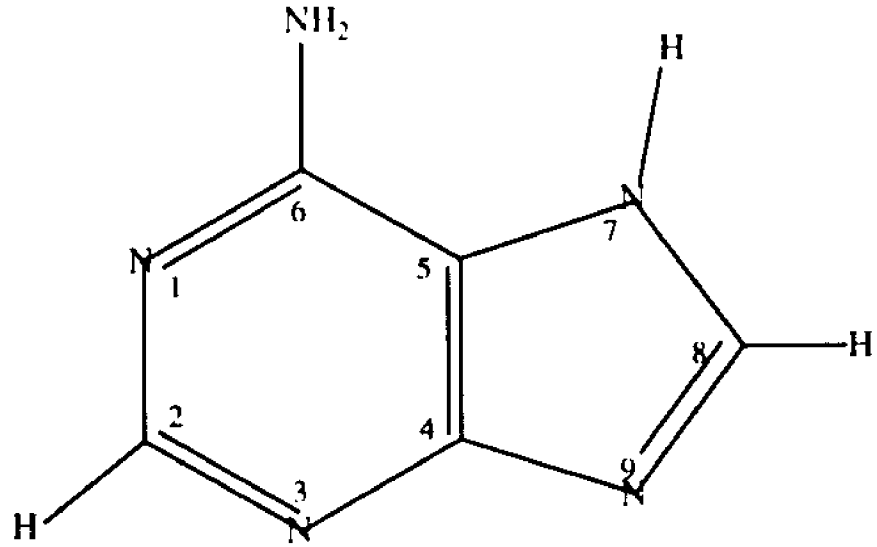

(b)

Figure 4.1

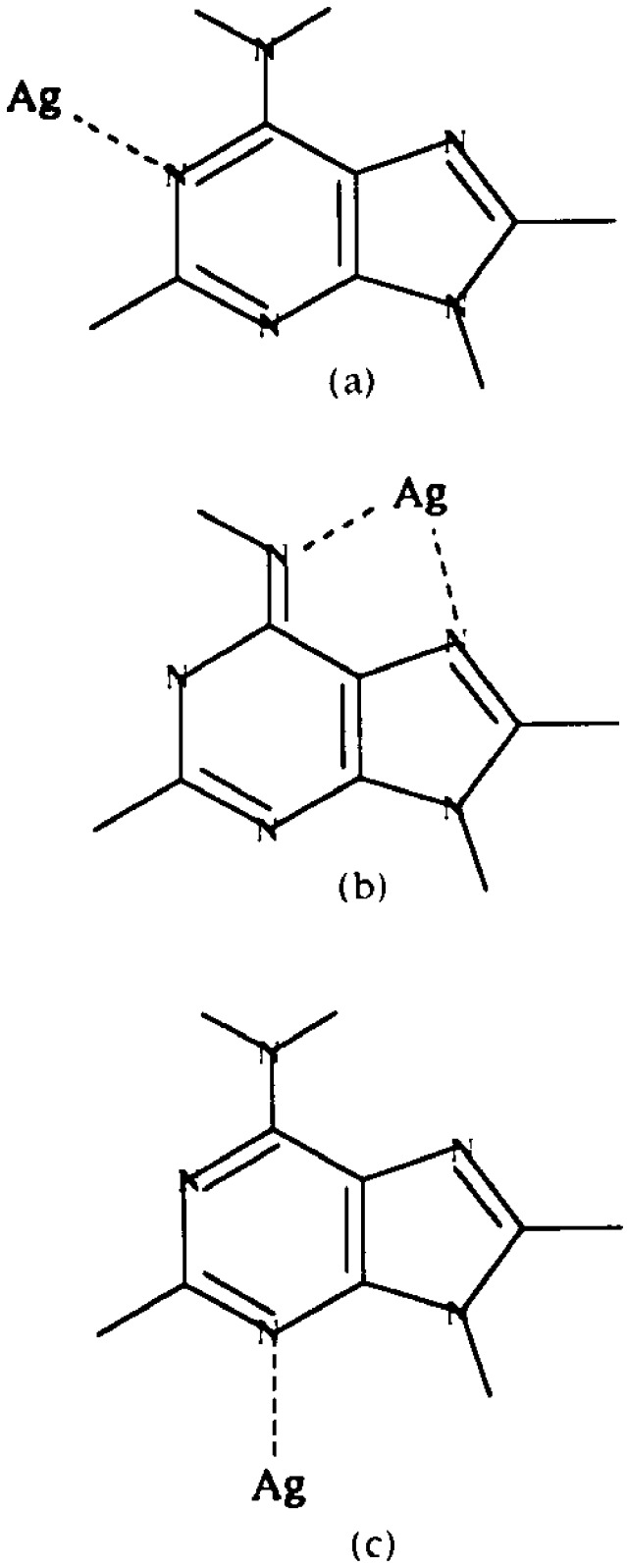

Figure 4.2

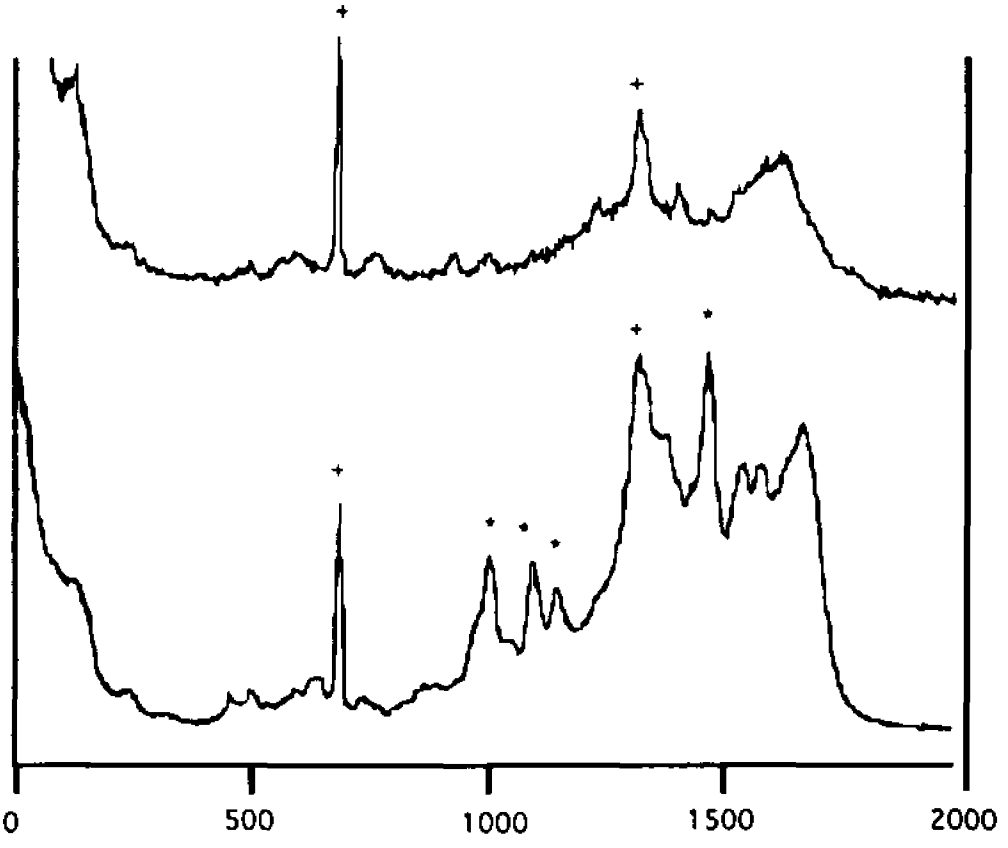

Figure 4.3(a)

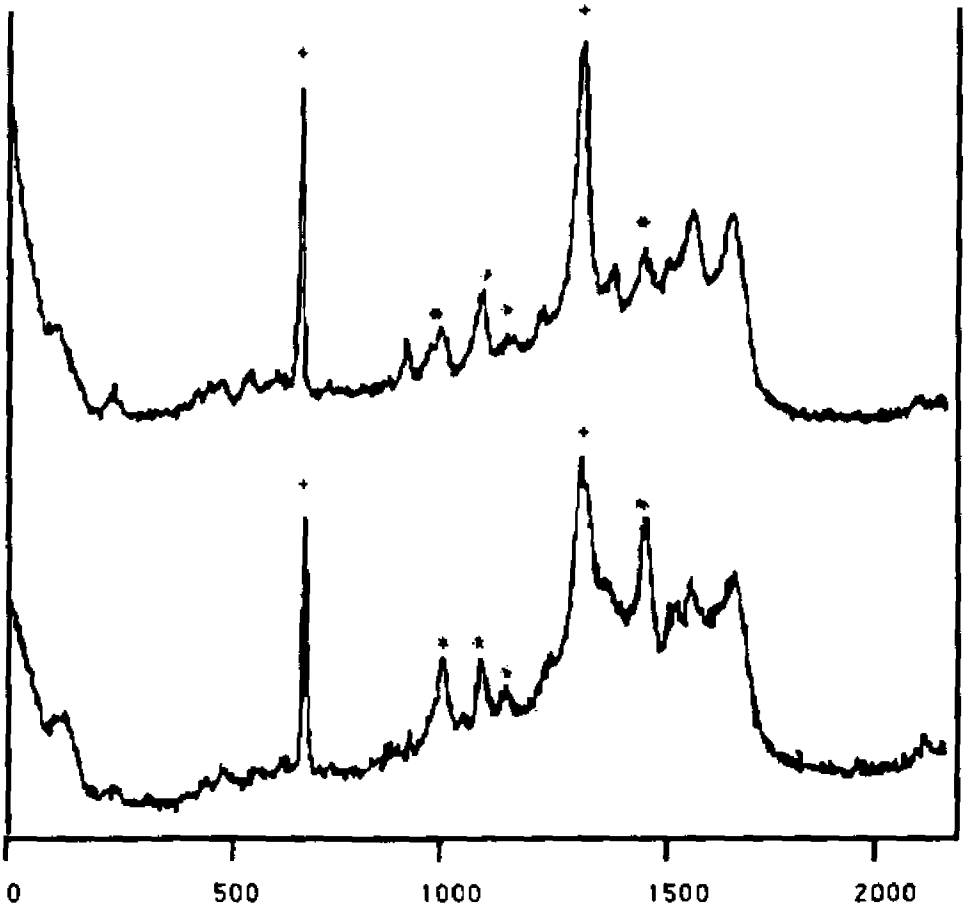

Figure 4.3(b)

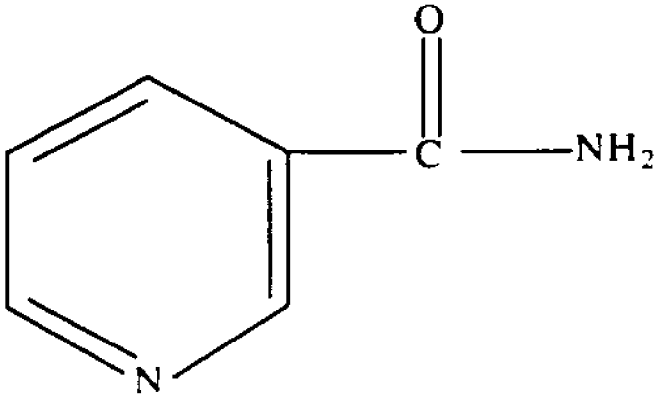

Figure 4.4

Chapter V: Normal Mode Calculations of 4-Atoms Clusters

5.1 Introduction

4-atoms clusters are interesting systems to study from the point of view of normal modes because their simplicity and high symmetry enables one to do the calculation with few parameters. The large number of electrons make quantum mechanical calculations of these systems somewhat difficult. However, Honea *et al.*[1] succeeded in doing *ab initio* calculations of a Si_4 cluster. In these studies, we first reproduced Honea *et al.*'s results and then calculated the normal modes of P_4, Bi_4 and Ta_4 based on these results.

5.2 Input files

The set of normal coordinate programs of Diem[2] was used in these studies. Table 5.1 shows sample data for a tetrahedral structure in the CINP.DAT file. Column NO assigns a number to an atom. Columns NO and NA define the distance between atoms in the same line. The distance is specified in column R. Columns NO, NA and NB define an angle between the atoms in the same line. The angle value is specified in

column TE. Finally, the first four columns define a dihedral angle between the planes defined by columns NO, NA, NB and NA, NB, NC. The value of the dihedral angle is specified in column PH.

Figure 5.1a shows atoms 1-4 from table 5.1 with reference to the xyz axis. Atoms 1, 2 and 4 are on the xy plane. Atom 3 is behind the xy plane. The line between atoms 2 and 3 represents the intersection of the planes defined by atoms 1, 2, 3 and 2, 3, 4. The data in table 5.1 was set up such that changing the dihedral angle from 70.53° to 180.0° (figure 5.1b) one can reproduce all the geometries between tetrahedral and rhomboidal. The 70.53° is obtained by subtracting the tetrahedral angle, 109.47°, from 180.0°.

The BINP.DAT defines internal coordinates of the molecule being studied. For 4-atoms clusters we use only bond stretches, each atom being bonded to three other atoms. The force constant values are entered in the NINP.DAT file in a one dimensional array. Each bond stretch may have its own element in the NINP.DAT file. However, bonds that are equivalent can be assigned the same element. The ZMAT.DAT file assigns the force constant values from NINP.DAT to the internal coordinates defined in BINP.DAT. Assigning the same force constant value to equivalent bonds insures that the proper symmetry of the modes will be reproduced. This is also the recommended way to assign force constants when using an optimization program.

5.3 Force Field Calculation

The Cartesian coordinates and the force constants matrix, $\mathbf{F}_x$, in mass weighted Cartesian coordinates of Honea *et al.* in Si_4 calculations were obtained from personal correspondence. The force constants were converted to internal coordinates using the expression

$$\mathbf{F}_x = \mathbf{B}^t \mathbf{F}_{ic} \mathbf{B} \qquad (1)$$

The **B** matrix was calculated the usual way with the BMAT.FOR program. The $\mathbf{F}_{ic}$ elements were obtained by fitting the calculated frequencies from these author's $\mathbf{F}_x$ matrix. The restricted simplex method explained in chapter II was used for the optimization. The force constants and observed frequencies are presented in tables 5.2 and 5.3 respectively.

Pre-assignment conditions were imposed during the optimization to keep the normal modes from crossing over each other. From the atomic displacement vectors, figure 5.2, one sees that force constant K(1-4) is most active in the totally symmetric modes (figures 5.2b and 5.2d) Pre-assigning K(1-4) to these modes insured obtaining the proper symmetry. All stretches around the ring were assigned the same value. The short cross-ring stretch was varied independently since it is shorter than the other ring bonds. All possible interaction parameters were used. The initial force constant values were obtained by fitting the frequencies by trial and error.

One other condition had to be imposed during the optimization. After transforming through equation (1), element $\mathbf{F}_x(7,4)$ was allowed to vary only within 0.5 % from the value of Honea *et al*. Trial runs showed that the error in this element was consistently out of proportion with the rest. Table 5.4 shows the two sets of $\mathbf{F}_x$ elements.

The force constants in internal coordinates obtained by the process described above were converted back to mass weighted Cartesian coordinates so as to compare them with the values of Honea *et al*. Although the errors are small, the converted values are not absolute since the uncertainty increases as the ratio of parameters to frequencies increases.

This method of transforming the force constants was effective for Si_4, but it is not recommended for large molecules. A direct transformation *via*

$$\mathbf{F}ic = \mathbf{B}\ \mathbf{F}_x\ \mathbf{B}^{\dagger} \qquad (2)$$

was tried without success. In order for this transformation to work, $\mathbf{B}$ has to be orthonormal. An orthonormalization program was written using the Gram-Schmidt algorithm. But the method failed after orthonormalizing the first 4 columns of the matrix.

To carry out a simplex optimization, it is best to have less parameters than frequencies being fitted. Several combinations of parameters were tried for Si_4. Table 5.2

shows the force fields that gave the best results with the least parameters. From the table, one notices that the stretching force constants depend on the choice of interaction parameters.

The cluster symmetry simplifies the tetrahedral force field. There are only 3 possible parameters, namely, bond stretch, stretch-stretch interaction between adjacent bond, stretch-stretch interaction between non-adjacent bonds. Table 5.2 also shows the results of optimizations of P_4, Bi_4 and Ta_4. A perfect frequency match was used as criterion for determining the proper force field.

5.4 Discussion

Table 5.5 shows the stretching force constants obtained with the simplex optimization and compares them with other methods. Somayujulu[3] used the formula

$$k_{AB} = (k_{AA} \cdot k_{BB})^{1/2} - \Delta$$

where k's are force constants between combinations of atoms A and B and Δ is an ionic contribution term. This formula can be applied to molecules other than diatomics. Ozin and McIntosh's method consists of multiplying the diatomic force constant by a fraction determined by the number of atoms in the cluster.[4] Although designed for diatomics, calculations

using Badger's rule are also shown.[5] The simplex optimization has the advantage over the other methods of reproducing accurately the experimental frequencies.

On calculating force constants of silver metal clusters, Ozin and McIntosh assumed that bonds with no atoms in common had no interaction, that bonds forming an acute angle had a negative interaction and those forming an obtuse angle had a positive interaction. No such patterns are observed in the simplex optimization results. Trial simplex runs showed that deviations from the force fields here presented yielded a less than perfect match.

Table 5.1. Sample CINP.DAT file for a tetrahedral cluster. Column labels are the same as used by Diem.

NO	NA	NB	NC	R	TE	PH
1						
2	1			2.250		
3	2	1		2.250	60.0	
4	3	2	1	2.250	60.0	70.53

Table 5.2. Si_4, P_4, Ta_4 and Bi_4 force constants. Simplex (a) and (b) are optimized results obtained with different parameters.

	Si_4			P_4	Ta_4	Bi_4
Force const.*	Honea *et al.*	simplex (a)	simplex (b)			
K(1-2)	1.6492	1.4867	1.5797	2.0661	1.8425	0.8926
K(1-4)	1.7578	1.4867	1.5797			
K(2-3)	0.0317	0.4446	0.1797			
$f_{1,2}$	-0.0221	-0.1854	-0.0924	-0.1215	0.0212	-0.0508
$f_{1,3}$	-0.3078	-0.0673	-0.1630			
$f_{1,4}$	-0.0028					
$f_{1,5}$	0.0703	-0.0930				
$f_{1,6}$	0.1632		0.0930	0.0942	0.0171	0.0005
$f_{3,4}$	0.1407					

* K are stretching force constants; f, interaction parameters. Numbers in parenthesis correspond to the atom numbers in figure 1 F's subscripts correspond to the following bonds: 1) 1-2, 2) 1-3, 3) 1-4, 4) 2-3, 5) 2-4, 6) 3-4.

Table 5.3. Observed frequencies of rhomboidal Si_4 and tetrahedral P_4, Ta_4 and Bi_4.

Si_4*	P_4**	Ta_4†	Bi_4‡
463	606	270	150
440	465	185	120
337	363	131	90

* From ref. (1)

** From ref. (7)

† From ref. (8)

‡ From ref. (9)

Table 5.4. Elements in the $\mathbf{F}_X$ matrix from Honea *et al.* and those reproduce with the simplex.*

Element	Honea *et al.* value	Simplex value	% difference
1,1	2.4321	2.4309	-0.049
4,1	-1.1485	-1.1479	0.052
6,1	0.7860	0.7858	-0.025
7,1	-1.1485	-1.1479	0.052
9,1	-0.7860	-0.7858	-0.025
10,1	-0.1351	-0.1352	-0.074
3,3	2.0025	2.0024	-0.005
4,3	0.4420	0.4415	-0.113
6,3	-0.3804	-0.3801	0.079
7,3	-0.4420	-0.4415	0.113
9,3	-0.3804	-0.3801	0.079
12,3	-1.2418	-1.2422	0.032
4,4	2.2551	2.5232	-0.075
7,4	-0.2281	-0.2274	0.307
10,4	-1.1485	-1.1479	0.052
12,4	-0.4420	-0.4415	0.113

Table 5.4. Continued.

6,6	0.8815	0.8613	-0.023
9,6	-0.1008	-0.1011	-0.298
10,6	-0.7860	-0.7858	0.025
12,6	-0.3804	-0.3801	0.079
7,7	2.5251	2.5232	-0.075
10,7	-1.1485	-1.1479	0.052
12,7	0.4420	0.4415	-0.113
9,9	0.8615	0.8613	-0.023
10,9	0.7680	0.7858	-0.025
12,9	-0.3804	-0.3801	0.079
10,10	2.4321	2.4309	-0.049
12,12	2.0025	2.0024	-0.005

* $\mathbf{F}_x = \mathbf{B}^\dagger \mathbf{F}_{ic} \mathbf{B}$, where $\mathbf{F}_x$ is the Cartesian coordinates force constant matrix, $\mathbf{F}_{ic}$, the internal coordinate force constant matrix and **B** the transformation matrix between the two.

Table 5.5. Comparison of force constants obtained through different methods.

Element	Simplex	Honea *et al.*	Somayaju-lu	Ozin & McIntosh	Badger
Si_4	1.5797	1.6492	2.064		0.9096
P_4	2.0661		1.854	1.852	1.374
Ta_4	1.8424				
Bi_4	0.8926		0.44	0.6133	

Figure Captions

Figure 5.1(a) Tetrahedron described by data in table 5.1.

Figure 5.1(b) Squared planar figure formed by opening the dihedral angle though bond 1-4.

Figure 5.2 In plane normal modes of square planar Si_4. Calculated frequencies in cm^{-1} are: (a) 500, (b) 463, (c) 440, (d) 337, (e) 288.

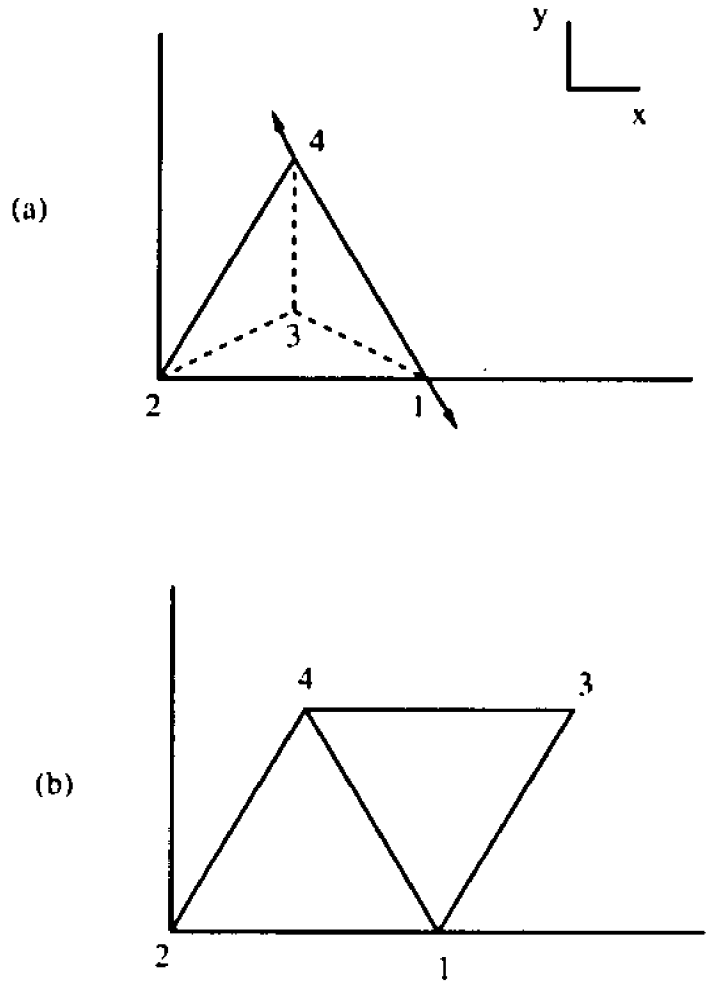

Figure 5.1

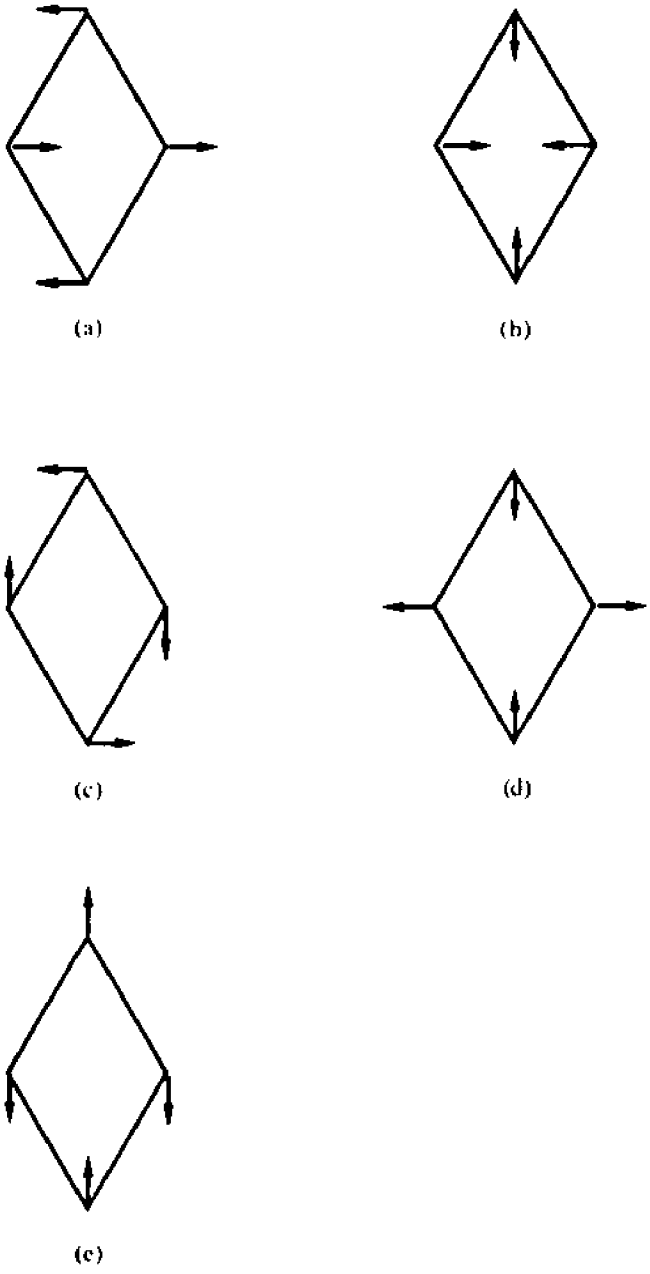

Figure 5.2

Appendix: Simplex Instructions

The simplex method is used for optimizing the parameters of a multi-dimensional function. A simplex is a geometrical figure defined by one more than the number of the function parameters The method works by evaluating the function at the vertices of the simplex, comparing the results, discarding the worst value and tracing a new vertex from the discarded one. The process is repeated until the best value is found.

A Nelder-Mead[1] simplex was adapted to the normal coordinate programs from Diem.[2] This author modified the Schachtschneider[3] programs for PC use. One advantage that the set of programs from Diem has over other normal coordinate programs is that it allows for Urey-Bradley force field calculations. The Nelder-Mead simplex was modified to enable one to impose conditions on the iterations thereby avoiding specious results. Following are the instructions for the use of the simplex program and a general description of its workings. They are meant to go along and compliment Diem's programs and instructions.

The diagonalization of the force constant matrix in the NOCO.FOR program yield the calculated frequencies, potential energy distribution and the atomic displacement vectors. The simplex compares the frequency fit of each iteration on the basis of the average percentage error as given by NOCO.FOR. The conditions imposed on each iteration consist of pre-

specifying (or pre-assigning) the main contributing force constant or group of force constants for any normal mode. After each diagonalization, the program checks the conditions in the PED and discards the solution that does not meet the requirements. The assignments are usually obtained from experimental data, namely, isotopic substitutions and comparisons with similar molecules. Some researchers have based the assignments on *ab initio* calculations. Not all assignments need be known prior to the calculation. In fact, one important use of the normal coordinate calculation is to help make the assignments.

The simplex routine uses the same input files needed for NOCO.FOR with some changes for two of them, CONTROL.DAT and NINP.DAT. In the CONTROL.DAT file, three new parameters are added at the end of the original row. The first added parameter specifies the number of force constants that will be considered in the conditions evaluation. This feature is useful for eliminating a group for force constants from the conditions evaluation, *e. g.* the non-bonded interactions. The program will check in the NINP.DAT file from the force constant 1 to this number only. The force constants in the NINP.DAT file should thus be ordered accordingly. The other two new parameters in the CONTROL.DAT file are tolerance parameters. The first of these is the number of iterations needed for the results to be improved by the second one. The simplex will stop whenever these requirements are not met. Generally speaking, if after 100 iterations the results have

not improved by 0.001 Å, they will not improve much further. However, each molecule and force field is different and it usually takes some tinkering with these numbers to get good results.

Several changes were made to the NINP.DAT file. After the force constant descriptions, a column of integers was added.

4.968771	K(C-H)	2	0.7500
5.996109	K(N-C)	3	0.7500
5.315372	K(C-C)	3	0.7500

These are labels for separating the force constants into groups, *i.e.*, hydrogen stretches, ring deformations, etc. The members of a group will be given the same number. After these integers, another column was added. This column determines the size of the increment—or step—of each force constant when constructing the initial simplex. The step is the product of the force constant and this number. It is added or subtracted to the starting force constant according to the sign of the number. As a rule of thumb, when far from the minimum, these parameters may be around 0.75; near the minimum, around 0.25. It is often fruitful to make the steps for the off-diagonal forces larger than those of the diagonal ones. This is because they are usually smaller and their values do not transfer directly from molecule to molecule.

Rows of six integers follow each frequency. The first column specifies the type of condition evaluation. The others specify the force constants assignments.

1242.0	1	4	5	6	0	0
1142.0	2	3	0	0	0	0
1098.0	0	8	9	0	0	0

There are four types of condition evaluations. They are specified by the numbers 1 through 4. A 1 in the first column means that one of the force constants in the following columns has to be the main contributor in that frequency. A 3 means that any of the following force constants has to be at least the second major contributor. A 4 means that any two of the following force constants have to be the main two contributors. A 2 in the first column is used for group assignments. As already mentioned, the numbers after the force constant description are labels that affix the force constants to a groups. While calculating the PED, the program will add the contributions from the force constants with the same label and compare the totals. One of the groups in columns 2 through 7 has to be the main contributor. This feature is useful when the main contributing group is known, but not the specific force constant. For example, the ring stretches in pyridine are known to be the major contributors to the frequencies in the 1500 cm^{-1} region. Yet, it is difficult to know specifically before hand which is the main

stretching for each frequency. A zero in the first column skips to the next frequency. This feature may be used when the assignment of a frequency is uncertain.

Before running the simplex, the frequencies are made to match the known assignments. This is done with the NOCO.FOR program as described in Diem's instructions. After the match is obtained, the simplex is set to run. Depending on the molecule and the force field, the simplex may go through anywhere between 100 to 2000 iterations before reaching a minimum. Many times, the simplex gets trapped in a local minimum. For these cases, the program is set up to self-start again using the best force constant values from the previous run. The simplex has two output files. FC.OUT gives the best set of force constant values for each simplex run. SMPLX.OUT gives the best values for the last run.

The whole optimization program is composed of several sub-programs. The main program, SIMPLEX.FOR, constructs the initial simplex , stores force constant values in FC.OUT and calls subroutines READDAT and AMOEBA. READDAT reads the data from BMAT.DAT, ZMAT.DAT and NINP.DAT. AMOEBA does the force constants variations and calls function FAMOEB for the results. FAMOEB in turn calls subroutine CALC where the force constant matrix diagonalization takes place. CALC was adapted directly from NOCO.FOR. It returns an average percentage error. FAMOEB returns this value to AMOEB for further processing while storing in SMPLX.OUT the best values for the

run. The other subroutines, MAZERO, MAPRO, and NDIAG, are called by CALC just as in NOCO.FOR.

While the simplex is running, the computer screen will show: NS, NK, NI, ITER. NS is the number of the current simplex run. NK is the number of times the diagonalization has been done. NI is related to the tolerance parameters from CONTROL.DAT. It is the difference between NI and ITER that has to surpass the tolerance parameter for the simplex to stop. ITER is the number of iterations. On the screen, there will also be AV. PR. This is the average percentage error of each calculation. LOWEST PERCENTAGE is the best value from the previous simplex run.

The program may be stopped at any time since the best values are being continuously stored. The information on the screen should help in deciding how long to let the program run. For a molecule like methylchloride, good results may be obtained in 100 iterations. Pyridine may require up to a thousand iterations and may take several hours depending on the computer. To obtain the final results, the output from FC.OUT and SMPLX.OUT is copied as is on to NINP.DAT for a NOCO.FOR run.

Ending with a word of caution, the simplex optimization will not give absolute values. Neither is it a panacea, *i.e.* the simplex will not always find the best solution automatically, even with the restrictions, nor will it always correct a defective starting force field.

References

Chapter I

1) E. B. Wilson, J. B. Decius and P. C. Cross, *Molecular Vibrations*; McGraw-Hill: New York, **1955**.

2) J. H. Schachtschneider, *Vibrational Analysis of Polyatomic Molecules*; Shell Development Company Report, Emeryville, CA, **1964**.

3) M. Diem, D. F. Burow, *J. Chem. Phys*. **1976**, 64, 5179.

4) R. L. Birke, J. R. Lombardi, *Spectrochemistry: Theory and Practice*; Plenum, **1988**.

5) G. Herzberg, *Molecular Spectra and Molecular Structure*; Van Nostrand Reinhold Co.; New York, **1945**.

6) G. M. Barrow, *Introduction to Molecular Spectroscopy*; McGraw-Hill New York, **1962**.

7) K. Nakamoto, *Infrared and Raman Spectra of Inorganic and Coordination Compounds* ; John Wiley & Sons, New York, **1986**.

8) M. Diem, *Introduction to Modern Vibrational Spectroscopy*; John Wiley & Sons, New York, **1993**.

9) H. C. Urey and C. A. Bradley, *Phys. Rev.* **1969**, 38, 1969.

10) T. Simanouti, *J. Chem. Phys.* **1949**, 17, 245.

11) S. N. Deming and S. L. Morgan, *Anal. Chem.* **1973**, 43, 278A.

Chapter II

(1) J. Overend and J. R. Scherer, *J. Chem. Phys.*, **32**, 1289 (1960).

(2) J. Overend and J. R. Scherer, *J. Chem. Phys.*, **32**, 1296 (1960).

(3) J. Overend and J. R. Scherer, *J. Chem. Phys.*, **1960**, 32, 1720.

(4) J. Overend and J. R. Scherer, *J. Chem. Phys.*, **1960**, 33, 446 .

(5) T. Simanouti, *J. Chem. Phys.*, **1949**, 17, 245.

(6) T. Simanouti, *J. Chem. Phys.*, **1949**, 17, 743.

(7) T. Simanouti, *J. Chem. Phys.*, **1949**, 17, 848.

8) S. N. Deming and S. L. Morgan, *Anal. Chem.* **1973**, 43, 278A.

9) Quantum Mechanical Exchange Program, University of Indiana, Bloomington, IN. (QMAC003)

10) D. A. Long, R. B. Gravenor and M. Woodger, *Spectrochim. Acta* **1963**, 19, 937.

11) G. Zerbi and S. Sandroni, *Spectrochim. Acta* **1976**, 24A, 511.

12) M. Diem, D. F. Burow, *J. Chem. Phys.* **1976**, 64, 5179.

13)X-Y Li, M. Z. Zgierski, *J. Phys. Chem.*, **1991**, 95, 4268.

14) A. Barlow and M. Diem, *J. Chem Ed.*, **1991**, 68, 35.

15) W. H. Press, B. P. Flannery, S. A. Teukolsky and W. T. Vetterling, *Numerical Recipes* Cambridgr University Press, New York, **1985**.

16) J. H. Schachtschneider, *Vibrational Analysis of Polyatomic Molecules;* Shell Development Company Report, Emeryville, CA, **1964**.

17) G. Herzberg, *Molecular Spectra and Molecular Structure;* Van Nostrand Reinhold Co.; New York, **1945**.

18) E. B. Wilson, J. B. Decius and P. C. Cross, *Molecular Vibrations;* McGraw-Hill: New York, **1955**.

19) M. Diem, *Introduction to Modern Vibrational Spectroscopy;* John Wiley & Sons, New York, **1993**.

20) M. Abe and Y. Kyogoku, *Spectrochim. Acta* **1987**, 43A, 1027.

21) H. Susi and J. S. Ard, *Spectrochim. Acta* **1974**, 30A, 1843.

22) J. C. Evans, *Spectrochim. Acta* **1960**, 16, 428.

23) J. R. Scherer and J. Overend, *Spectrochim. Acta*, **1961**, 17, 719.

24) M. Tsuboi, *Spectrochim. Acta* **1960**, 16, 505.

25) F. Milani-Nejad and H. D. Stidham, *Spectrochim. Acta* **1975**, 31A, 1433.

26) G. Pongor, G. Fogarasi, I. Magdó, J. E. Boggs, G. Keresztury and I. S. Ignatyev, *Spectrochim. Acta* **1992**, 48A, 111.

27) S. Susuki and W. J. Orville-Thomas, *J. Mol. Struct.* **1977**, 37, 321.

28) A. R. Katritzky and C. W. Rees, *Comprehensive Heterocyclic Chemistry*, Pergamon Press, Oxford, 1984.

29) X.-Y. Li, R. S. Czernuszewicz, J. R. Kincaid, Y. O. Su and T. G. Spiro, *J. Phys. Chem.* **1990**, 94, 31.

30) R. M. Badger, *J. Chem. Phys.* **1933**, 2,128.

31) R. M. Badger, *J. Chem. Phys.* **1935**, 3, 710.

32) M. Majoube, *J. Raman Spectrosc.* **1985**, 16, 98.

Chapter III

1) R. L. Birke, J. R. Lombardi, *Spectrochemistry: Theory and Practice*; Plenum, **1988**.

2) M. Moskovits, *Rev. Mod. Phys.* **1985**, 57, 783.

3) D.-S. Wang and M. Kerker, *Phys. Rev.* **1981,** B24, 1777.

4) J. R. Lombardi, R. L. Birke, T. Lu and J. Xu, *J. Chem. Phys.* **1986,** 84(4), 4174.

5) M. Fleishman, P. J. Hendera and A. J. McQuillan, *Chem. Phys. Letters* **1974,** 26, 163.

6) A. L. Vivoni, J. R. Lombardi and R. L. Birke, to be published.

7) J. R. Lombardi, E. A. Shields Knight and R. L. Birke, *Chem. Phys. Letters* **1981,** 79, 214.

8) K. A. Bunding, R. L. Birke and J. R. Lombardi, *Chem. Phys.* **1980,** 54, 115.

9) G. C. Pimentel and A. L. McClellan, *The Hydrogen Bonding,* Freeman, New York, **1960**.

10) L. A. Sanchez, J. R. Lombardi and R. L. Birke, *Chem. Phys. Letters* **1984,** 108, 45.

11) K. Nakamoto, *Infrared and Raman Spectra of Inorganic and Coordination Compounds* ; John Wiley & Sons, New York, **1986**.

12) W. Biemolt, G. J. C. S. van de Kerkhof, P. R. Davies, A. P. J. Jansen and R. A. van Santen, *Chem. Phys. Letters* **1992**, 188, 477.

13) J. A. Rodriguez and C. T Campbell, *Surface Sci.* **1988**, 194, 475.

14) P. S. Bagus and K. Hermann, *J. Chem. Phys.* **1984**, 81, 1965.

15) M. Majoube, *J. Raman Spectrosc.* **1985**, 16, 98.

16) L. Pauling, *The Nature of the Chemical Bond;* Cornell University Press, **1960**.

17) D. L. Jeanmaire and R. P. and Duyne, *J. Electroanal. Chem.* **1977**, 84, 1.

18) J. A. Creighton, *Surface Sci.* **1983**, 124, 209.

19) R. Dudde and E. E. Koch, *Surface Sci.* **1986**, 178, 646.

20) S. Susuki and W. J. Orville-Thomas, *J. Mol. Struct.* **1977**, 37, 321.

21) S. Susuki, *J. Mol. Struct.* **1982**, 86, 387.

22) R. P. van Duyne, *Chemical and Biochemical Applications of Lasers*, Vol. 4, Academic Press, New York, **1979**.

23) J. F. Evans, M. G. Albrecht, D. M. Ullevig and R. M. Hexter, *J. Electroanal*. **1980**, 106, 209.

24) R. Dornhaus, R. E. Buener, R. K. Chang and H. Chabae, *Surface Sci*. **1980**, 101, 367.

25) F. R. Dollish, W. G. Fateley and F. F. Bentley, *Characteristic Raman Frequencies of Organic Compounds* ; John Wiley & Sons; New York, **1974**.

26) J. A. Rodriguez, *Surface Sci*. **1992**, 273, 385.

27) M. Moskovits and D. P. Dilella, *J. Chem. Phys*. **1980**, 73, 6068.

28) M. Moskovits, *Chem. Phys. Letters* **1983**, 58,

29) G. Herzberg, *Molecular Spectra and Molecular Structure;* Van Nostrand Reinhold Co.; New York, **1945**.

Chapter IV

1) O. Siiman, R. Rivellini, R. Patel, *Inorg. Chem.* **1988**, 27, 3940.

2) J. C. Austin, R. Hester, *J. Chem. Soc., Faraday Trans.* **1989**, 85(5), 1159.

3) C. Otto, F. F. M. de Mul, A. Huizinga, J. Greve, *J. Am. Chem. Soc.* **1988**, 92, 1239.

4) M. Majoube, *J. Raman Spectrosc.* **1985**, 16, 98.

5) A. Hirakawa, H. Okada, S. Sasagawa, M. Tsuboi, *Spectrochim. Acta* **1985**, 41A, 209.

6) M. J. Nowack, L. Lapinski, J. S. Kwiatkowski, J. Leszczynski, *Spectrochim. Acta* **1981**, 47A, 87.

7) J. R. Lombardi, E. A. Shields Knight and R. L. Birke, *Chem. Phys. Letters* **1981**, 79, 214.

8) K. T. Yue, C. L. Martin, D. Chen, P. Nelson, D. Sloan, R. Callender, *Biochem.* **1986**, 25, 4941.

9) A. R. Katritzky and C. W. Rees, *Comprehensive Heterocyclic Chemistry*, Pergamon Press, Oxford, 1984.

10) R. C. Lord and G. J. Thomas Jr., *Spectrochim. Acta* **1967**, 23A, 2551.

11) Z. Dhaouadi, M. Ghomi, J. C. Austi, R. B. Girling, R. E. Hester, P. Mojzes, L. Chinsky, P. Y. Turpin, C. Colombeau, H. Jobic and J. Tomkinson, *J. Phys. Chem.* **1993**, 97, 1074.

Chapter V

1) E. C. Honea, A. Ogura, C. A. Murray, K. Raghavachari, W. O. Sprenger, M. F. Jarrold and W. L. Brown, *Nature* **1993**, 366, 42.

2) A. Barlow and M. Diem, *J. Chem Ed.*, **1991**, 68, 35.

3) G. R. Somayajulu, *J. Chem. Phys.* **1958**, 28, 814.

4) G. A. Ozin and D. F. McIntosh, *J. Phys. Chem.* **1986**, 90, 5756.

5) R. M. Badger, *J. Chem. Phys.* **1933**, 2,128.

6) P. D. Dilella, W. Limm, R. H. Lipson, M. Moskovits and K. V. Taylor, *J. Chem. Phys.* **1982**, 77, 5263.

7) C. S. Venkateswaran, *Proc. Ind. Acad. Sci.* **1935**, 2A, 260.

8) H. Wang, R. Craig, H. Haouari, J.-G. Dong, Z. Hu, A. Vivoni, J. R. Lombardi and D. M. Lindsay, *J. Chem. Phys.* **1995**, 103(9), in press.

9) V. E. Bondybey and J. H. English, *J. Chem. Phys.* **1980**, 73, 42.

Appendix

1) S. N. Deming and S. L. Morgan, *Anal. Chem.* **1973**, 43, 278A.

2) M. Diem, D. F. Burow, *J. Chem. Phys.* **1976**, 64, 5179.

3) J. H. Schachtschneider, *Vibrational Analysis of Polyatomic Molecules;* Shell Development Company Report, Emeryville, CA, **1964**.